Advances in Science and Technology Research Journal

Advances in Science and Technology Research Journal, 2026, 20(2), 212–242
https://doi.org/10.12913/22998624/210041
ISSN 2299-8624, License CC-BY 4.0

Received: 2025.10.15
Accepted: 2025.05.22
Published: 2025.12.23

Method for precision automatic unbalance control in wind turbines by continuously adjusting correction mass

Łukasz Breńkacz[1*], Rafał Rumin[2], Jędrzej Blaut[3]

[1] Faculty of Management, AGH University of Krakow, Antoniego Gramatyka 10, 30-067 Kraków, Poland
[2] Institute of Fluid Flow Machinery, Polish Academy of Sciences, Fiszera 14, 80-231 Gdańsk, Poland
[3] Faculty of Mechanical Engineering and Robotics, AGH University of Krakow, al. Adama Mickiewicza 30, 30-059 Kraków, Poland
* Corresponding author's email: lukasz.brenkacz@imp.gda.pl

ABSTRACT

This publication describes the analysis of a method for precision automatically balancing an offshore wind turbine by continuously changing the correction mass. The motivation for this work was to make wind turbines safer and extend their service life. Automatic balancing has never been used in wind turbines, and this article aims to show the potential of this method in wind turbines. The presented balancing concept is based on using fluid as a correction mass for balancing. Wind turbine blades are subject to icing, which results in an additional mass of ice covering their surface. Its effect can be reduced by adding or removing correction fluid from individual turbine blades to compensate for imbalance mass. In this way, correction systems mounted on the shaft of the wind turbine have been used. The proposed solution can be used to perform wind turbine balancing, where the correction elements are placed inside the turbine blade. As part of the simulation study, analyses were performed on a 5 MW offshore wind turbine model using MADYN 2000 software. A beam model was created using the finite element method and service loads were specified. On the basis of the wind turbine, appropriate correction masses were given to reduce the vibration amplitude level to acceptable values. Fatigue analysis deepens understanding of the impact of imbalance on the longevity of turbine components, pointing toward potential pathways to extend their life and improve safety. The use of an automatic balancing system will extend the service life, improve the safety of wind turbines, and increase their efficiency.

Keywords: rotor, vibration reduction, rotordynamics, automatic balancing, wind turbine, health monitoring, offshore engineering.

INTRODUCTION

Renewable energy sources have been in development since the 1990s. The authors' motivation to introduce automatic wind turbine balancing is for several reasons. Incorporating sustainable development principles into wind energy projects is essential to ensure environmental and economic benefits throughout the life cycle of wind turbines. This includes not only the operational phase, but also manufacturing and end-of-life management. A comprehensive approach to sustainability in wind energy includes a responsible source of raw materials, minimizing environmental impact during production, and developing the strategies to recycle and reuse turbine components at the end of their useful life (1). The wind turbine production phase involves the extraction and processing of raw materials, which can have significant environmental impacts. Research suggests that advances in material science and manufacturing processes can reduce these impacts by improving the efficiency of material use and reducing the carbon footprint of production (2, 3). Furthermore, optimizing the design for durability and recyclability can further improve the sustainability of wind turbines. For example, the use of composite materials that can be separated and recycled at the end of

their life cycle is gaining traction in industry (4). During the operational phase, the implementation of automatic balancing systems, as discussed in this article, contributes to sustainability by extending the service life of wind turbines as well as reducing the need for frequent maintenance and replacement of parts. This not only reduces the operational carbon footprint, but also reduces the environmental impact associated with the manufacture and transport of replacement parts (5).

The imbalance increases fatigue loads in the blades, tower, increasing drivetrain, and thus fatigue damage and frequency of noncritical failures, leading to downtime and economic losses. As a part of the failure, the turbine blade can be damaged (6), which can cause the blade to break off the structure (7). Furthermore, this phenomenon could be dangerous, because a detached turbine element can fly away over a distance of several hundred meters. Therefore, research has been carried out in the field of finding the methods to improve the reliability of wind farms. One of the solutions considered is the automatic wind turbine balancing system proposed for the first time in this study during operation.

The cause of damage to rotating machinery is the uneven distribution relative to the rotation axis. Imbalances can be caused by manufacturing errors, as well as rotor blade aging processes, manifested by changes in the profile of the rotor blade or the appearance of erosion on the surface of the rotor blade (8). Unbalance caused by rotor blade icing is a separate problem (9). Even small unbalanced masses can cause dynamic loads that affect the operation of wind turbines (9, 10). The vibrations caused by imbalances can have a large vibration amplitude. The result of wind turbine failure is downtime, which in an offshore environment due to complex logistics results in a large increase in wind farm maintenance costs (7).

The standard balancing procedure checks the vibration of the tower as the rotor blades rotate close to the nominal speed:

1. The vibration is measured when the turbine rotor is rotated at a speed equal to 80–90% of the first natural frequency of the tower.
2. Measurement of vibration after adding trial correction mass to one of the rotor blades.
3. Estimation of the imbalance based on two previous vibration measurements.

In wind turbines, unbalance is a very important topic. Approximately 20–50% of wind turbines have significant rotor imbalances (11). This leads to damage to important components. Imbalances influence the long-term operation of wind turbines. There are two main causes of imbalances: the so-called mass imbalance resulting from non-uniform mass distributions caused, for example, by manufacturing inaccuracies or water inclusions in the blade texture and aerodynamic imbalance resulting from errors in inclination angles or blade change profiles. Aerodynamic imbalance is not necessarily erroneous, but it also occurs during normal operation. Due to turbulence, wind shear, yaw misalignment, vertical wind profile, and tower shadow, there are always differences in the lift forces between the blades, which result in imbalanced forces on the turbine, like mass imbalances. In addition to lateral vibrations, they induce axial and torsional vibrations in wind turbines. The main reason for the aerodynamic imbalance is the relative deviation of the blade pitch angles. This can be eliminated only by correcting these angles. Additional masses are not helpful. In practice, both types of imbalances are frequently observed, both separately and in combination.

In general, we do not have an influence on the correction during wind turbine operation. For the numerical calculation, the maximum imbalance value for the machine class was obtained according to the relevant standard (12, 13). Methods are known for the continuous determination of imbalance during rotating machinery operations that can be used in condition monitoring systems (CMSs). These methods use the modeling of rotating machines using basic geometric and physical parameters (11). These parameters and their values were described in Chapter 6. A well-balanced rotor is essential for the long-term and safe operation of wind turbines. The problem of excessive rotor vibration is related not only to imbalance, but also to different blade angles or blade aerodynamic imbalances. Cacciola et al. (14) developed a sophisticated control algorithm to compensate for mass imbalance by generating additional counteracting aerodynamic imbalance with individual pitch control. Obtaining the maximum output from a wind conversion system also requires optimization of the rotor speed to wind speed. This article discussed the results of numerical analysis and the design of a structural solution to build an automatic balancing system for a wind turbine.

An imbalance is a source of vibration with rotational frequency. Rotor imbalance causes

additional periodical forces at the frequency of once per revolution (1P), which excites the blades, tower, and drivetrain and can be observed in the frequency spectrum of different vibration sensors. To determine the imbalance class according to the standard (standard number ISO 1940-1), a vibration acceleration measurement was carried out using accelerometers. Accelerometers are commonly connected to the bearing supports of the main shaft; also, the rotational speed must be known. This type of measurement is sent to an acquisition system, such as the SCADA system. On the basis of these signals, it could be assessed, for example, whether the imbalance is too high to be acceptable.

Scientific papers seeking more accurate methods for determining the angle and mass of the imbalance have used eddy currents or inductive displacement sensors. (15, 16). It is also possible to determine the imbalance using current and voltage analyses. In (17), a support vector machine was used to determine the magnitude and angular position of the imbalance based on current and voltage signals. (18) proposed a method to detect the imbalance of the blades of marine hydrokinetic (MHK) turbines based on several statistical indicators from the signal of a shaft key encoder. The method was verified using a numerical model. Acceleration sensors (accelerometers) are mostly used for vibration detection under industrial conditions. An exception is the diagnostics of slide bearings, where the information on the operating stability of a slide bearing is realized by predictors based on an analysis of the shaft rotation trajectory relative to the bearing. To record rotation trajectories, it is necessary to obtain the information about relative vibrations, which can only be achieved by measuring the relative distance from the shaft to the sensor (19). Sensor signals were recorded by condition monitoring systems (CMS), conditioned, and analyzed. Usually, the detection of imbalances is based on spectral and order analysis methods (20). Another technique is to monitor the characteristic of the power (21), where mean values are observed and deviations from faultless conditions are used to calculate alarm limits. However, this requires a learning phase under faultless conditions (22). This holds also for other signal processing methods. Another disadvantage is that the amount of imbalance, for example, the absolute value and location of a mass imbalance or the deviation of one or more pitch angles, is not computable. The state-of-the-art in rotor imbalance determination still requires an on-site expert team. Aerodynamic imbalances must be detected using optical methods. After aerodynamic imbalances, the mass imbalance was determined using vibration measurements with and without reference masses. In recent years, the authors have developed the methods that allow determination using the data collected by a CMS. Consequently, the amount and location of the rotor imbalance can be computed without expensive measurements using on-site reference masses. Niebsch et al. presented an algorithm to experimentally calculate the mass and aerodynamic imbalance of wind turbines (23). Several procedures are known to detect an increase in imbalance and new methods are being developed. CNN has been used, among others (24). It is also possible to use the signal in a narrower frequency range, (25) complex Morlet wavelet transform (26) or the Teager -Kaiser Energy operator (27).

Johnson et al. (28) published an article in which they balanced fatigue damage and turbine performance through an innovative pitch control algorithm. To improve reliability, marine conditions require expensive and advanced systems. Emergency systems are constantly being developed to avoid danger to people and harm to the environment (29). In addition to emergency systems, numerical methods are being developed to allow the diagnosis of machines operating under varying environmental conditions. For example, row analysis synchronized with shaft rotation allows one to determine single-number statistical parameters (30). Numerical methods based on the analysis of nonlinear phenomena, such as the Teager-Kaiser Energy operator (27), are currently being developed. Recent advances in mechanical system diagnostics include the application of dispersion entropy with a sliding window technique, which enables an effective assessment of system stability by capturing the complexity and variability of vibration signals in both linear and nonlinear dynamic regimes (31, 32). The methods for analyzing the effect of operating pressure on the natural frequencies of the equipment were presented in (33). In the developed auto-balancing method, calibration is performed by filling the selected correction tanks. This provides a readout of the signal with and without the additional correction mass. This makes it possible to identify the signals originating from a mass imbalance

and isolate signals originating from another phenomenon (e.g., aerodynamic imbalance).

Larger wind turbines are more advantageous from the developer's point of view, because installation and internal wiring costs depend mainly on the number of wind turbines, rather than their size. Increasing the scale of turbines is also beneficial as a result of the costs of operation and maintenance. In terms of wind farm energy production, larger wind turbines are characterized by fewer individual machines that require maintenance. This results in lower operating and maintenance costs. However, these costs are directly dependent on failure rates, part costs, and the time it takes technicians to perform each maintenance task. This is why they increase with the size of the wind turbines. A study was conducted using a discrete event simulation model for the operational phase of an offshore wind farm, comparing the operation and maintenance costs of a wind farm consisting of 5 MW turbines with a wind farm consisting of 10 MW turbines (34). The simulation results confirm that the operating and maintenance costs decrease when replacing two 5 MW turbines with a 10 MW turbine, provided that the total production capacity and all other parameters are the same (35). The operation and maintenance of offshore wind turbines play an important role in the development of offshore wind farms (36).

The operation process of an offshore wind farm is extremely complex. Offshore wind energy requires the selection of a maintenance strategy that considers scheduling, which is an optimization problem that considers on-site operations, repairs, evaluation criteria, recycling, and environmental issues (37). Wind turbine operating cost planning is more complex for offshore farms than onshore farms. Offshore farms increase projected costs by 9.6%, while offshore farms increase projected costs by 1.7% (38).

Reliability analyses show a decrease in the reliability of the power system in the case of the transition from nuclear power to smaller distributed renewable power plants (39). Reliability studies have shown that even a five-fold increase in power plant capacity (for example, 3.480 MW) using renewables is less reliable than a nuclear plant (for example, 696 MW) (40). According to the reliability studies conducted for offshore wind turbines, the most prone to failures is the support structure (3.5 failures per year), followed by the auxiliary system (1.7 failures per year), pitch system (1.4 failures per year), generator (0.97 failures per year) and gearbox (0.32 failures per year). Failures are typically caused by harsh environmental conditions. The next causes are operational factors, aging, and material damage (41).

IMBALANCE OF ROTORS AND WIND TURBINES

Imbalance in the rotors is an undesirable phenomenon; therefore, various methods are used to reduce this imbalance. This process is called rotor balancing and is achieved by adding or removing a certain amount of mass from the rotor disc in the appropriate planes. This should be performed in such a way that the center of mass lies on the axis of rotation. Static and dynamic balancing for the rotors must be performed. Static imbalance of a rotor is a condition in which its principal axis is displaced parallel to its rotational axis. In a dynamically unbalanced rotor, the rotor axis and its central principal axis of inertia are oblique, and the center of gravity does not lie on the rotor axis.

Equilibrium equations of moments (for centrifugal forces due to imbalances) (42). The given equations are more general and can be used for multiplane balancing. In practice, balancing is performed in only one plane.

Types of imbalance

In rotating machinery, specific linear and angular accelerations generate inertial forces. According to the principle of d'Alembert, these forces are transmitted to the bearing supports through various mechanisms, such as rolling or sliding bearings, streams of gases or liquids, magnetic fields, or electric fields (43). Periodically varying loads can lead to several adverse effects, including component vibrations, fatigue stresses, excessive bearing wear, casing and foundations, and environmental noise. These vibrations can arise during machine operation due to wear and tear of parts, or manufacturing errors. The key factors causing vibrations include friction, centrifugal forces, fluid forces within seals and bearings, as well as the elastic properties of the shaft, its supports, and bearings. To mitigate these undesirable phenomena, the balancing of machine elements is applied. Balancing is done by changing the mass of the rotor disc in the appropriate plane so that the center of gravity is on the axis of rotation (the main central axis of inertia). Both static and

dynamic rotors are comprehensively balanced, either on their own bearings or in special balancing machines. In recent research, an automatic ~~balance~~ rotor balancing device was developed. For this system, a mathematical model of a rigid rotor was adopted. This model treats the shaft as a "rigid body" element and considers the two bearing supports as compliant. This simplification enabled effective modeling of the rotor and performance simulations using the MSC ADAMS software. This type of rotor design allows direct vibration measurements on the bearing body, facilitating more accurate analysis and adjustments. Balancing is a critical practice in rotordynamics to ensure smooth operation and longevity of rotating machinery. By developing advanced tools and models, such as the automatic balance device and the rigid rotor model, engineers can better predict, measure, as well as mitigate the adverse effects of vibrations, improving the overall performance and reliability of these systems.

A mathematical equation was initially derived to determine the reaction forces that act on the bearings (Figure 1). The rotating wheel spins with an angular velocity ω around the Z axis and has an angular acceleration ε (43). Rotation (1) of the rotor creates dynamic reactions in the bearings, which depend on the position of the rotor's principal central inertia axis relative to its axis of rotation. When a thin layer of thickness *dz is isolated* within the rotor (an infinitesimally small element with mass *dm* can be considered. This mass *dm* experiences an elementary centrifugal force *dF* and an elementary tangential force dF_1.

$$\begin{aligned} d\bar{F} &= dm\omega^2\bar{r}, \\ d\bar{F}_1 &= dm(\bar{\varepsilon} \times \bar{r}) \end{aligned} \tag{1}$$

where: F – centrifugal force, F_1 – peripheral force, ω – angular velocity on the Z axis of the rotor, ε – angular acceleration about the Z axis of the rotor, r – position vector of the center of mass, m – mass of the rotor.

By defining (2) the coordinates of the center of mass dm through the components x, y, it can be stated that the position vector is: r = xi + yj, for unit vectors i, j.

Substituting the position vector into the above formulas, we obtain dF and dF1 after calculating the cross product:

$$\begin{aligned} d\bar{F} &= dm\omega^2(x\bar{\imath} + y\bar{\jmath}), \\ d\bar{F}_1 &= dm[\bar{\varepsilon} \times (x\bar{\imath} + y\bar{\jmath})] = dm\bar{\varepsilon}(x\bar{\imath} + y\bar{\jmath}) \end{aligned} \tag{2}$$

where: x, y coordinates of the center of mass; i, j – unit vectors.

Taking into account inertial forces, the dynamic reactions in the bearing can be written as an integral over volume V of the rotating body (3):

$$R_B = \iiint_V \frac{[\![(d\bar{F}]\!] + d\bar{F}_1)z}{L} \tag{3}$$

where: dz – elementary layer of thickness dz has been isolated in the rotor, z – distance from the bearing to the elementary section, L – distance between bearings, R_A, R_B – dynamic reactions of both bearings.

By substituting dF and dF1 with the formula defined by the x, y coordinates, we obtain (4) (43):

$$R_B = \frac{1}{L}\begin{bmatrix} (\omega^2\bar{\imath} + \varepsilon\bar{\jmath}) \\ \iiint_V \; xzdm + (\omega^2\bar{\imath} - \varepsilon\bar{\jmath}) \\ \iiint_V \; yzdm \end{bmatrix} \tag{4}$$

When the centrifugal moments of the rotor with respect to the x and y axes are equal to zero,

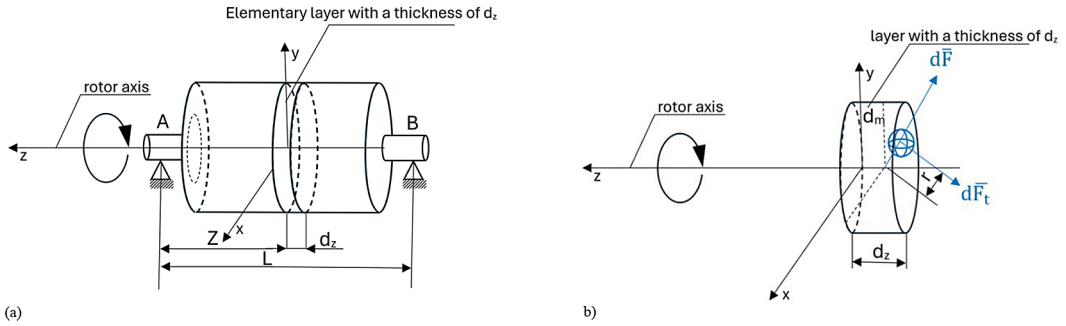

Figure 1. The diagram shows an example of a rigid rotor (a) and the division of the rotor (b) into a section with a thickness marked with the variable *dz*

then the reaction on the rotor bearings is zero, and the axis is its principal axis of inertia.

$$\iiint_V xzdm = 0\,,$$
$$\iiint_V yzdm = 0\,.$$

In the case where the resultant value of the normal and tangential inertial forces is equal to zero, the dynamic reactions of both bearings are zero (5):

$$\begin{gathered} R_B = R_A = 0, \\ \iiint_V (d\bar{F} + d\bar{F}_t) = 0\,, \\ (\omega^2\bar{\imath} + \varepsilon\bar{\jmath}) \iiint_V xdm + \\ +(\omega^2\bar{\imath} - \varepsilon\bar{\jmath}) \iiint_V ydm = 0 \end{gathered} \tag{5}$$

The equation above is satisfied when the rotor axis passes through the central axis of inertia (the center of gravity of the rotor).

$$\iiint_V xzdm = 0\,,$$
$$\iiint_V yzdm = 0\,.$$

This means that then the rotor has no dynamic reactions in the bearings and it is called a perfectly balanced rotor.

Most rotating machines operate at speeds outside their resonant frequencies; therefore, vibrations reach limited values. However, the rotor often passes through successive natural frequencies during acceleration or deceleration, which exposes it to the appearance of an increase in vibration amplitude. A change in imbalance can be caused by a change in mass distribution as a result of a change in operating conditions, such as dust adhering to the blower blades or ice build-up on the blades of the wind turbine (10). The vibration that occurs limits the life of the equipment and the cyclic nature of the vibration causes fatigue loading, which can cause a break of the turbine blade (44). One way to reduce the negative impact of resonance is to use active foil bearings (45). Then, it is possible to change the frequency of resonance occurrence. Wind turbines do not use active bearings; therefore, minimizing the effect of imbalance is a critical task to enable proper operation.

Rotor balancing methods

Despite careful balancing of the rotors during the manufacturing stage, residual vibrations often emerge once the rotor is installed in its operating environment. This phenomenon results from assembly tolerances, interactions with the support structure, or changes in mass distribution during service. For these reasons, various in situ balancing techniques have been developed to correct for imbalance directly on the machine's own bearings (46).

The necessity of in situ balancing arises particularly in two cases:

- when rotors are too large to be balanced on conventional balancing machines, which is common in turbomachinery,
- when progressive wear or degradation of the rotor components alters the mass distribution over time, thereby generating new unbalance conditions.

Among the multiplane balancing approaches performed on their own bearings, two fundamental groups of methods can be distinguished (46, 47).

- Modal methods.

Modal balancing is designed specifically for flexible rotors, where shaft deflections under centrifugal forces play a significant role. In such cases, unbalanced forces not only generate vibrations, but also induce elastic deformations of the shaft, which modify the overall mass distribution of the system (46).

A distinctive feature of flexible rotor dynamics is that deflection patterns are speed-dependent. At any given rotational speed, the shaft deflection is a superposition of multiple modal shapes. When the rotor operates near its critical speed, the response is dominated by the shape of the r-mode, which must be taken into account when applying balancing corrections (47).

Therefore, modal balancing focuses on reducing vibration amplitudes associated with specific modal components of the response. This approach is particularly effective in high-speed turbomachinery, where shaft flexibility cannot be neglected and rigid-body balancing methods prove insufficient.

- Influence coefficient methods (46–48).

The influence coefficient method is one of the most widely used techniques for balancing rigid rotors directly in their operational bearings. Its principle is to determine how sensitive the measured vibration response is to the placement of a trial mass in a given correction plane. This sensitivity is expressed through influence coefficients, which form a linear relationship between unbalance forces and measured vibrations.

The method relies on the following assumptions (46, 47):

- The measured vibration response is linearly dependent on the rotor imbalance.
- The rotor behaves as a rigid body within the operating speed range under consideration.
- During the measurement process, the mass distribution remains constant, except for the addition or removal of the trial masses.

The balancing process consists of two main phases: a measurement stage and a computational stage. In the first phase, a set of vibration measurements (amplitude and phase) is performed: initially for the uncorrected rotor and then for successive runs with trial masses placed in different balancing planes. In the second phase, these data are used to calculate the necessary correction mass and its angular position using the linear influence relation (48) :

$$V_i = U_i \cdot H_{ii} + U_j \cdot H_{ij} \tag{6}$$

where: V_i – vibration vector measured at the i-th observation point, U_i, U_j – vectors of unbalance forces acting in the ii-th and jj-th correction planes, H_{ii}, H_{ij} – influence coefficients representing the sensitivity of vibrations to correction masses applied in the respective planes.

The main advantage of the influence coefficient method is that it does not require detailed prior knowledge of the dynamic model of the system, making it a broadly applicable and practical approach. In principle, an effective correction can be achieved in four main steps, using only vibration measurements and trial masses. However, several drawbacks must be noted. The method requires multiple shutdowns and restarts of the machine (typically four), which prolongs the balancing process. Furthermore, placing test masses without precise knowledge of the system may inadvertently introduce additional imbalance, leading to an increase in vibration levels rather than their reduction (46–48). Finally, this method is restricted to the rotors that can be treated as rigid bodies, limiting its applicability in the case of flexible high-speed rotors.

Examples of imbalance

An example of an imbalance that occurs during rotor operation is air handling equipment (fans and blowers) that supplies particulate-contaminated air to the furnace. During fan operation, dust particles stick to the rotor blades or other components of the fan, which can cause an imbalance.

Examples of imbalances were also observed in wind turbines (Figure 2). Wind turbines operate under various climatic conditions around the world. However, adapting their operation to a given climate also requires analyzing the impact of ice-split deposition on turbine blades, especially when the equipment operates at temperatures below 0 °C, such as under high mountain conditions. In extreme cases, the amount of ice accumulated on a turbine can be up to approximately half the weight of the blade itself (49) or approximately 25–30 kilograms per meter of the blade. This mass causes a significant disturbance to the wind turbine and prevents it from working properly. Bai et al. proposed the diagnosis of icing of wind turbine blades using RFECV-TSVM pseudo-sample processing of RFECV-TSVM (50).

A rotor heating system can be used to remove the top layer of the ice cover. This provides the operating conditions where a temperature of +4 °C is maintained on the surface of the blade. Temperature and humidity sensors are used to detect ice and compare the operating characteristics of the machine, because ice changes the aerodynamic properties of turbine blades, reducing the power generated by the turbine. To achieve the ice-melting effect, channels exist inside the blade to blow hot air over each blade, which requires approximately 85 kW of power for a single wind turbine. There are many active devices to remove ice, including resistance foils, heating the interior of the blade with hot air, dissolving the ice with electrical pulses or electrical separation, and using low-frequency ultrasound waves (52–57). However, producers are now working on the solutions to remove ice from blades with very low power consumption. These solutions

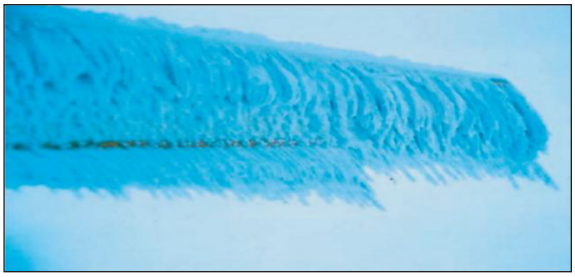

Figure 2. Accumulation of ice layers on wind turbine blades (51)

are used when there are human facilities around wind farms. For isolated objects, a fluid -based rotor balancing system can be used to balance the blades, which can effectively reduce vibrations caused by imbalance without exposing people to injury from a detached ice block.

Due to the uneven distribution of the ice in the individual blades, the entire turbine is unbalanced (58). An example of an iced wind turbine blade is shown in Figure 3a. The effect of imbalance involves periodically occurring vibrations that can contribute to damage to various elements, such as gears and blades. The materials from which turbine blades are made are based on epoxy or polyester laminates with glass or carbon fibers. These materials are lightweight and strong, but their fatigue strength is limited. Therefore, when exposed to repeated load cycles, they may break earlier than predicted under normal wind turbine operation (59). An example of a wind turbine blade failure is shown in Figure 3b.

Methods of balancing

Automatic rotor-balancing systems can be used to reduce imbalances during rotor operation. Feand and Cui [47] presented a risk assessment method using an auto-balancing mechanism (62). Imbalance correction is possible in real time while the machine is running. Some solutions are used in the industry for this purpose. Currently, there are no commonly used automatic balancing systems for wind turbines.

The first solution (Figure 4) involves generating a corrective force with two moving masses in the same plane moving under a fixed radius of the axis of rotation. The balancing process is based on the influence coefficient method and includes specific measurement and control solutions. The influence coefficients are determined in the first stage, which is then used to balance the rotor at a specific speed during its transient response to minimize vibration at critical speeds.

Another example is a system with two liquid chambers and heaters, in which a liquid is transferred from one chamber to the other by evaporation and condensation. Such devices are mainly used to balance large rotors in fans and blowers (49).

Recent progress in trial-weight-free model-based balancing shows promise in reducing outage time. Sanches et al. (63) augmented the state vector with unknown imbalance parameters and apply an augmented Kalman filter to identify the unbalance in a flexible rotor directly from operating responses; simulations and experiments demonstrate accurate identification without trial runs. However, the approach hinges on careful noise-covariance tuning and sufficient sensor observability, and has so far been validated on laboratory rigs, rather than multi-MW wind turbines; after estimation, the method still requires a physical actuation path to implement the correction.

Sun et al. (64) presented a model-based balancing method for multi-disc flexible rotors without trial weights, showing that a distributed unbalance can be approximated by equivalent isolated unbalances on selected planes and then identified via reduced-order models; two numerical case studies report ~80–98% vibration reductions of 80–98% after low- and high-speed correction. Practicality is tempered by sensitivity to model fidelity (e.g. bearing/foundation properties, reduction errors) and by the requirement that available correction planes align with actual unbalance locations, the conditions that can be difficult to guarantee in assembled wind turbine drivetrains.

(a) (b)

Figure 3. (a) Wind turbine blade after four days of intense ice formation (60), (b) photo of a wind turbine blade after failure in which a 5.5-meter tip fell from the blade (Korsze, Poland) (61)

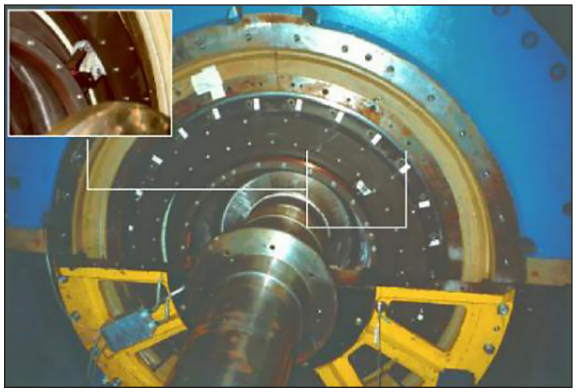

Figure 4. Example of a balancing disc

For online trial-weight-free correction, Yun et al. (65) developed a spray-based dynamic balancing system that identifies the imbalance via a no-test-weight algorithm and deposits precise corrective mass in situ; spindle tests show large (>70%) amplitude drops in seconds. While attractive for automated correction, the technique assumes ready access for material deposition and tight control of deposition accuracy and sealing, constraints that make direct transfer to utility-scale rotors and harsh nacelle environments nontrivial.

Addressing aerodynamic imbalance rather than mass imbalance, Bertelè et al. (66) proposed an automatic detection and correction of pitch misalignment using generator power and blade load signals, with a supervisory algorithm that compensates systematic blade-pitch offsets. Their field-motivated simulations showed reduced asymmetric loading without hardware modification, yet the strategy mitigated the effects of imbalance rather than eliminating the underlying mass asymmetry and relied on accurate sensor calibration and stationarity of the misalignment.

Complementary individual pitch control (IPC) schemes continue to evolve for load mitigation under imbalance. Zhang et al. (67) introduced a PI–R IPC that targets balanced and unbalanced 1P/2P load components in the hub frame and demonstrate significant reductions on the NREL 1.5 MW reference turbine using FAST simulations. As a control-side solution, IPC reduces fatigue drivers but does not correct rotor mass properties; its performance depends on actuator bandwidth, measurement quality, and may trade off against energy capture in turbulent inflow.

Building on the review above, current solutions leave a clear gap that motivates a fully automatic closed-loop mass-balancing system for utility-scale turbines. Classical field balancing requires trial masses, repeated stoppages, and quasi-steady conditions; inverse/model-based estimators identify imbalance but stop short of physically correcting it; CMS/SCADA-driven classifiers flag imbalance states without prescribing correction mass placement; and control-side remedies (IPC, pitch-misalignment compensation) mitigate effects rather than eliminate the underlying mass eccentricity. Emerging on-line actuators (e.g., deposition or discrete add-on devices) have shown rapid attenuation on spindles but face scalability, accessibility, and environmental constraints in nacelles. In response, this paper targeted an online, trial-weight-free approach that (i) continuously estimates both mass and aerodynamic imbalance under variable-speed, turbulent inflow using standard nacelle sensors (vibration, tachometry, and power) fused with a rotor-dynamic model and adaptive observers, and (ii) closes the loop by re-centering the rotor via a compact, continuously adjustable corrective-mass mechanism integrated in the hub/nacelle. The purpose was to maintain a low 1P/2P vibration and asymmetric loading throughout the operating envelope without shutdowns. Methodologically the estimation-and-actuation architecture was formulated, its stability and convergence properties were derived, and the performance on a representative drivetrain rig and high-fidelity simulations was evaluated. The novelty lies in combining fleet-deployable sensing, robustness to non-stationary excitation, and autonomous mass redistribution into a single system that diagnoses and corrects imbalance during normal operation.

AUTOMATIC ROTOR BALANCING SYSTEMS

The idea behind this concept was to use a correction disc with three or four fluid chambers, as shown in Figure 5. The accumulation of fluid in a given correction chamber made it possible to adjust the mass of the imbalance because the resultant correction mass depended on the degree of filling in each chamber (68). Each chamber was connected to an external hydraulic system through a hydraulic circuit, as well as the input and outlet valves. The use of valves allows for the filling and emptying of individual tanks to be regulated. Hydraulic accumulators were used as tanks. The automatic control system involves measuring the

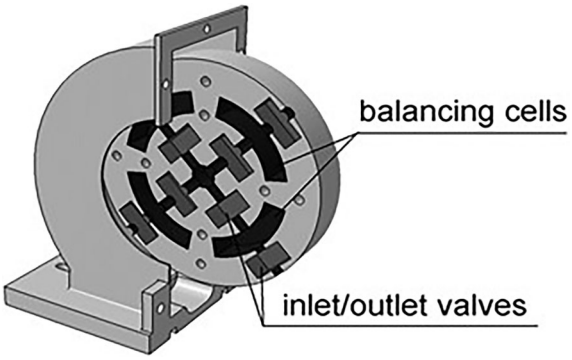

Figure 5. Schematic showing a correction disc with four correction chambers (70)

acceleration amplitude of vibration on the rotor bearings and adjusting the hydraulic filling level of the accumulators to reduce the system (69).

In further studies, the number of correction chambers was reduced to three pieces distributed around the disc every 120°, as this is the necessary number to balance a mass placed at any position of the plane of the correction disc. The research used the influence coefficient method to determine the resultant imbalance vector causing the imbalance centrifugal force "F" and to calculate a correction force "-F" with the same value and direction but opposite sense. The value of the correction force F was then converted to the fluid fill volume of the individual correction vessels. For this purpose, it is also necessary to determine the value of the phase-shift angle between the phase marker located at the starting point of the correction disc and the maximum measured value of the rotor vibration amplitude caused by the imbalance. Figure 6 shows a graph of the phase shift angle and rotor vibration amplitude measurement step.

The assumption that the rotor response is proportional to the imbalance is fundamental to virtually all balancing methods for both rigid and flexible rotors (42). Even for systems where substantial nonlinearity is observed, this assumption can be satisfied by balancing in a stepwise fashion with sufficiently small steps to approximate the linear behavior. An additional assumption inherent in most balancing methods, and of particular importance to influence coefficient balancing, is that the effect of individual unbalances can be superposed to give the effect of a set of unbalances. This has been generally accepted as a fact for unbalances that are not excessively large. The premise behind influence-coefficient balancing is that, based on these two assumptions, a rotor can be characterized by a set of individual trial-mass runs. This characterization can be used to define a combination of these masses that eliminates or minimizes the synchronous response of the rotor due to imbalance. The analytical development and implementation procedures for influence balancing are presented in the sixth chapter of Darlow's book (42). A method was also presented.

On the basis of the vibration amplitude and phase shift angle measurements, a vector plot can be obtained showing the centrifugal force F originating from the unbalanced mass, and the correction force -F originating from the filling of the correction fluid tank (Figure 7). Consequently, because the correction tanks were distributed around the correction disc every 120°, their positions were marked on the graph by lines X1, X2, and X3. Filling a given correction tank induces a centrifugal force (e.g. Fx2 and Fx3) originating from the mass of the correction fluid stored in the tank.

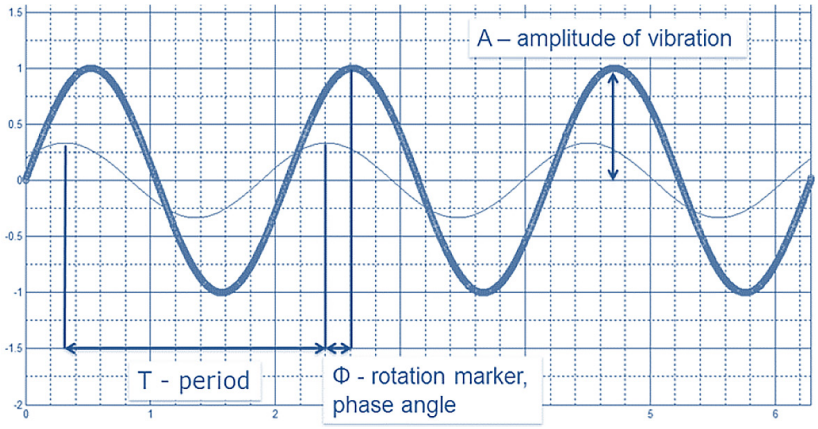

Figure 6. Measurement plot of the phase shift angle and the rotor vibration amplitude. The thick line (vibration sensor) represents the vibration amplitude, and the thin line is the rotation marker (based on (71))

On the basis of the assumptions made, multibody simulations (MBS) were performed using MSC ADAMS software (Automated Dynamic Analysis of Mechanical Systems) – as shown in Figure 8. The simplified target model was imported into the MSC ADAMS software after the bindings were added and the appropriate motions were specified. Then, in the bearing simulation, the measurement points of the forces corresponding to the rotor vibrations were completed in the simulation and a phase marker was added. Exemplary imbalanced forces were used in the simulation, and, for simplicity, the correction masses were replaced by parameterized force vectors. Owing to simulation limitations in MSC Adams, it was necessary to use the imbalance in the form of a force vector instead of the imbalance arising from a mass point. These two methods of setting the imbalance can be used interchangeably and produce similar effects. The prepared geometric model was linked to the MATLAB/Simulink software to develop a control system for the virtual prototype. To simulate the control system, the MSC ADAMS model was combined with MATLAB/Simulink software using a library to pass the input and output data between models.

As it was shown in Figure 8, a control system was used to reduce the rotor vibrations by appropriately changing the distribution of the correction masses. The influence coefficient method was used for this purpose. Vibration reduction was achieved by varying the force from the correction masses X1 and X3 to compensate for the X4 force from the imbalance example.

On the basis of the simulation results, a detailed correction disc was developed for the experimental tests (Figure 9). For this purpose, a correction disc was placed on the steel shaft. The hydraulic system used three AS 00 20 type hydro accumulators (as correction chambers) and six Lee Extended Performance (EP) microvalves to control the inlet and outlet of the correction chambers. The design of the correction disc is as follows:

Protection against the effect of free fluid movement can be realized independently of the rotational speed of the rotor. Therefore, a hydraulic accumulator should be used as a chamber for the correction liquid. The internal design of the accumulator should ensure the separation of the liquid from the compressed gas in such a way that the liquid that fills the accumulator accumulates at a specific location, with the possibility of expanding the volume of the accumulator filled with liquid. An important prerequisite for the correct operation of the system is the proper design of the diaphragm to separate the liquid from the compressed gas. (Figure 10). The correction chamber uses a hydroaccumulator (AS 00 20), which prevents the fluid from moving freely when the disc rotates.

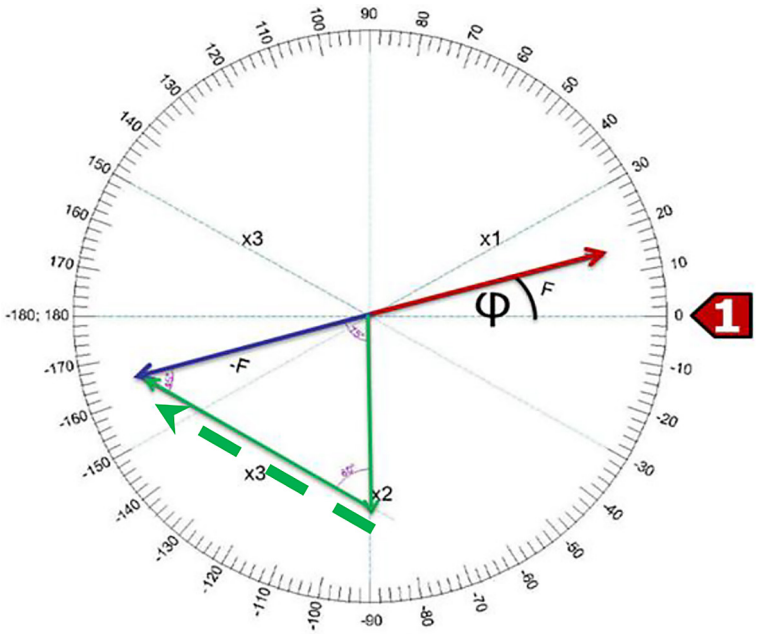

Figure 7. Correction disc with vector plot showing the centrifugal force "F" and the correction force "-F" derived from filling the correction fluid tank (based on (71))

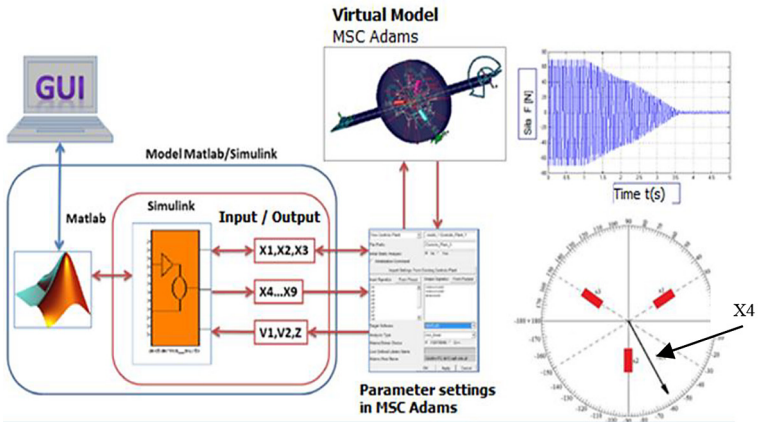

Figure 8. Schematic of co-simulation development in MSC ADAMS and MATLAB/Simulink software

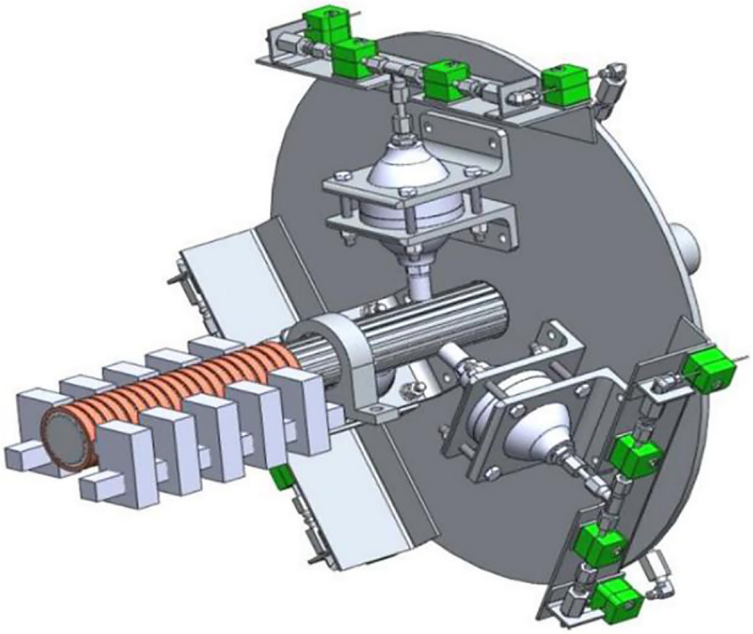

Figure 9. Correction dial design

As part of the experiment, the vibration amplitude measurements were performed using accelerometers mounted on the bearings of the rotor. An eddy current sensor was used to measure the rotational speed of the rotor. There was a phase-angle marker on the shaft in the form of a groove approximately 4 mm wide. An eddy current sensor for distance measurement was attached to the tripod to detect the position of the groove on the shaft. When the groove passed near the eddy current sensor, a signal appeared, indicating that the shaft had fully revolved. The experiments involved the use of filled hydroaccumulators as a correction mass and a mass that introduces an imbalance.

This balancing process can occur in several stages. In the first stage, the vibration amplitude and phase angle were measured. On the basis on their values, the angles and values of the correction mass to be supplied to the corresponding chamber on the correction disc were determined on the diagram. Next, the control buttons responsible for opening and closing the valves are activated manually. The hydroaccumulators are filled semi-automatically. Current measurements of the vibration acceleration amplitude were recorded on polar diagrams and a graph showing the change in these vibrations as a function of time.

The test rig, which was used to perform the measurements, consisted of the following components: a hydraulic system, a mechanical system, power supply system, and a control system.

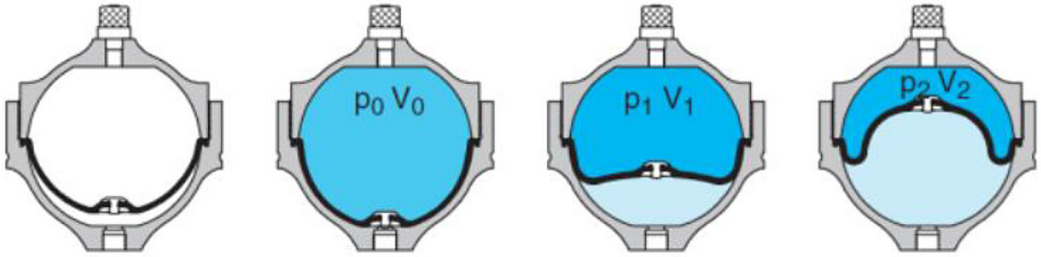

Figure 10. The correction chamber uses a hydroaccumulator (AS 00 20), which prevents the fluid from moving freely when the disc rotates (72)

The hydraulic system (Figure 11) is responsible for delivering the correction fluid (propylene glycol) from an external tank through a hydraulic pump and rotary hydraulic coupling. The correction fluid was distributed to individual correction chambers (hydro accumulators) using hydraulic tubes. The hydroaccumulator was filled with an inlet valve and emptied with glycol using an outlet valve. The mechanical system consists of a housing shaft, a correction disc, and holders for individual hydraulic components. The shaft was mounted on bearings that were held to the lab bench frame. The power and control system provided power and control signals via a slip-brush-type electrical connector located on the shaft. This solution is effective; however, the signals are subject to additional noise. The measurement system uses 3-axis accelerometers placed on the bearings and a phase marker in the form of an eddy current sensor placed perpendicular to the shaft axis. Valve control and measurements were performed using the LabView PXI controller.

Simulation and experimental results of the automatic balancing system

To assess the effectiveness of the proposed automatic rotor balancing system, both numerical simulations and experimental investigations were carried out. The combination of these approaches enabled the verification of the control algorithm in a virtual environment and subsequent validation of its performance on a laboratory test rig.

Since the MSC Adams software does not natively simulate free fluid motion, a simplified substitute model was introduced to preserve the key functional characteristics of the system. In the real setup, the corrective mass (fluid) is influenced by centrifugal forces, with three hydraulic accumulators evenly distributed every 120° around the balancing disc. In the numerical model, the corrective fluid was replaced by centrifugal force vectors, expressed as (1), where m is the corrective mass, r = 200 mm is the application radius, and ω is the angular velocity (0–2000 rpm). The model was integrated with Matlab/Simulink

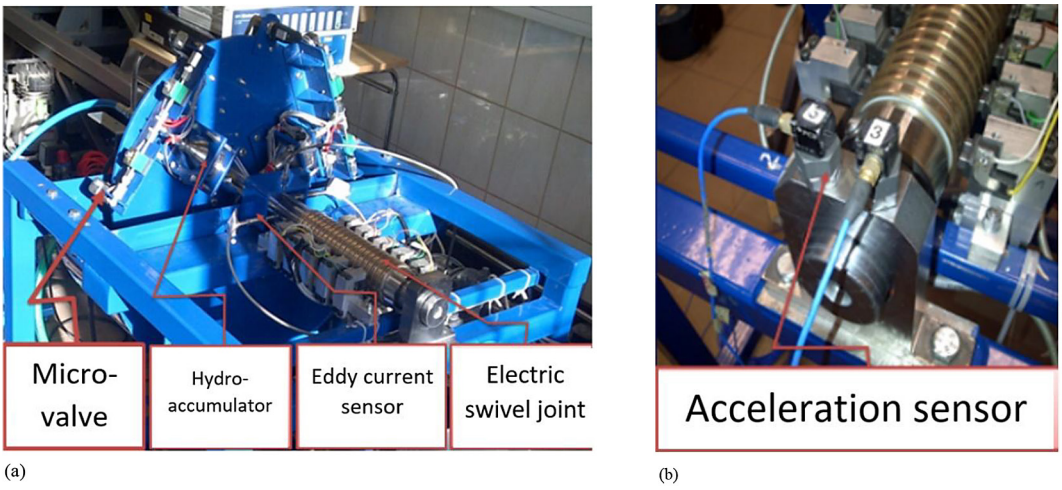

Figure 11. (a) Automatic rotor balancing process during experimental testing, (b) the measurement system uses 3-axis accelerometers placed on bearings

through a co-simulation interface, allowing real-time interaction between the dynamic simulation and the control system. The input variables represented the corrective forces applied in the three balancing chambers and the unbalance forces at selected angular positions, while the output signals included the vibration forces and the phase angle marker.

The implemented control algorithm successfully detected the amplitude and phase of the imbalance as well as calculated the appropriate filling ratios of the correction chambers. A test scenario with an unbalance force of 86 N at 210 ° relative to the phase marker showed that the system correctly identified the amplitude (85.91 N) and the phase (150 °). The corrective force was then distributed to the chambers, reducing the resultant imbalance from 85.91 N to approximately 8 N within 3 seconds of simulation time (Figure 12).

It should be noted that the simulation did not include the inertia of fluid flow within the chambers, which explains the short balancing time. Experimental studies provided complementary insight into these limitations.

Figure 13 shows the measurement results obtained by performing an automatic rotor-balancing experiment while the rotor was running at 900 rpm. The graph shows the acceleration amplitude measured with the accelerometer during the automatic balancing process. The system was originally unbalanced by adding an unbalanced mass, which caused rotor vibrations that were measured at an acceleration amplitude of approximately 3.75 mm/s2. The balance procedure was then started and the corresponding chambers were filled with correction fluid, causing the rotor to balance and reduce vibration to an acceleration amplitude level of approximately 1.25 mm/s2, which is the residual imbalance of the rotor. It should be noted that the jump in vibration amplitude occurring in the second 35 is caused by a momentary disturbance caused by the activation of the electrical system for controlling the operation of valves (this system generated disturbances at that moment but later did not affect the correctness of the measurement reading).

The combined results confirm the validity and effectiveness of the proposed system. The simulation model demonstrated the theoretical capability of rapid compensation of unbalance, reducing forces to near-zero levels in a few seconds. The experimental studies, although showing longer correction times due to fluid inertia, verified the system's ability to achieve substantial vibration reduction under realistic operating conditions.

The agreement between the simulation and the experimental results validates the detection as well as correction algorithms and demonstrates that the proposed approach can be implemented practically. The method ensures effective balancing while maintaining continuous rotor operation. Furthermore, the findings underline the potential

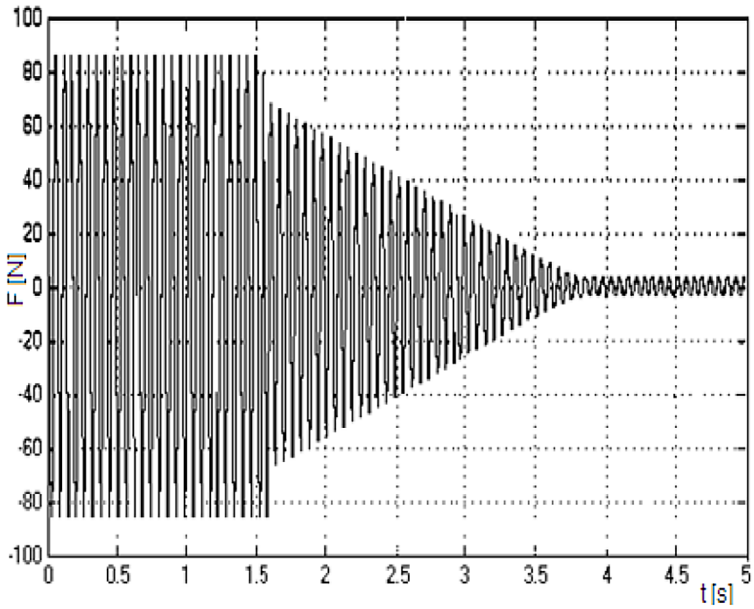

Figure 12. Reducing the resultant unbalance from 85.91 N to approximately 8 N within 3 seconds of simulation time: numerical calculations

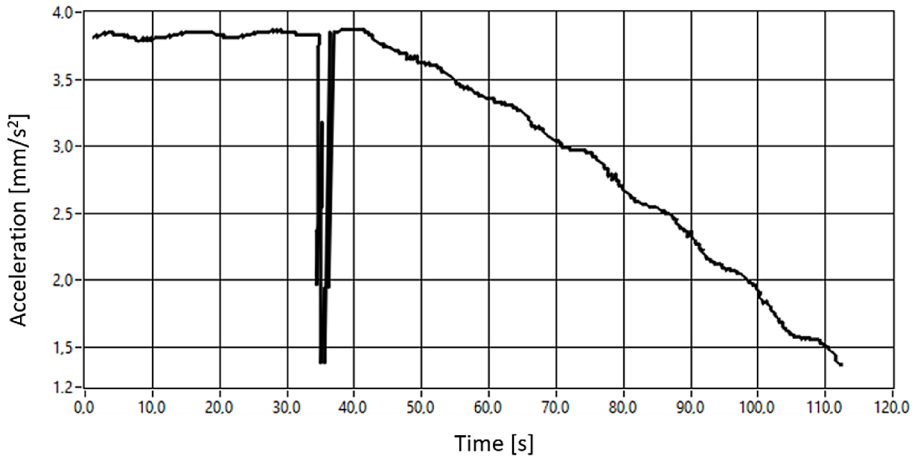

Figure 13. Result of experimental balancing

of applying such systems in industrial rotating machinery, particularly wind turbines, where automatic in-operation balancing could significantly improve reliability, extend component lifetime, and reduce maintenance costs.

Alternative rotor balancing strategies

Classical rotor-balancing practice in turbomachinery and machine tools remains dominated by influence coefficient and modal approaches that estimate correction masses/planes from phase-referenced vibration measurements taken during trial runs. Darlow showed that these families can be expressed within a unified framework, with clear guidance on selecting planes, iterating with trial weights, and handling flexible modes; however, they presuppose quasi-stationary operation and scheduled shutdowns for weight installation, which limits their applicability to large wind turbines operating under variable speed and turbulence (42). Complementing this, Foiles et al. reviewed decades of practice and documented practical shortcomings, such as multiplane coupling, repeatability under changing operating states, and the need for reliable phase references, which together motivate interest in the approaches that do not rely on repeated weight campaigns (73).

For compact spindles and consumer rotors, passive automatic ball/roller balancers redistribute free masses above a threshold speed to counteract eccentricity. Kim and Na designed a ball-type ABB that explicitly targets the well-known drawback of large transient 1× amplification of 1 during run-up, showing, in simulation and tests, how geometry and damping choices suppress transients while retaining steady-state benefits (74). Building on this, Van De Velde et al. (75) introduced a temporary speed-reduction procedure that statistically reduces residual scatter due to stiction, thereby improving repeatability across starts; their Journal of Sound and Vibration study provides quantitative gains and implementation guidance. While effective in controlled settings, these devices can amplify off-design transients and are hard to scale to multimegawatt drivetrains.

Another strand replaces mechanical bearings with actively controlled magnetic bearings to reject synchronous unbalance forces through control actions rather than mass add/remove. Herzog et al. (76) developed generalized notch-filter compensation embedded in multivariable feedback, demonstrating force-free rotation about the inertial axis while preserving closed-loop stability over speed. More recently, Noshadi and Zolfagharian (77) showed robust attenuation of unbalance and harmonic disturbances on a flexible shaft AMB rig using modern H / robust control, confirming that AMBs can traverse critical areas with attenuated 1× transmission – but at the expense of power electronics, backup bearings, and integration complexity atypical for conventional wind turbine drivetrains.

Machine-tool research demonstrates fully online active balancing, wherein the system identifies the resultant unbalance and actuates movable masses or metered fluid to the more recent mass in real time. Zhang et al. (78) proposed a liquid injection / free drip balancer and reported rapid vibration reduction (up to ~87% at test speed) without trial runs, illustrating that closed-loop identification/correction can be performed in hardware.

Hredzak and Guo (79) earlier presented an electromechanical ring with actively positioned balancing members as a compact actuator concept for variable imbalance. These concepts are promising, but face translation challenges to utility-scale wind turbines (environmental sealing, service access in nacelles, actuator energy/autonomy, and mass-metering accuracy at large radii).

In wind applications specifically, individual pitch control (IPC) can mitigate the asymmetric 1P/3P loads arising from rotor mass or aerodynamic asymmetries. Zhang et al. (67) proposed a PI-R IPC architecture in the hub frame and showed, via FAST simulations on the NREL 1.5 MW turbine that balanced and unbalanced components can be effectively attenuated with controller design alone. Subsequent wind energy studies have refined IPC and related yaw/pitch strategies, but these do not change the rotor mass properties; residual unbalance remains, and mitigation bandwidth can be limited by actuator authority and structural mode interactions.

Taken together, the prior art spans (i) trial-weight-based field balance that is robust but manual and intrusive (42,73); (ii) passive ABBs that excel at steady-state 1× suppression but suffer transient amplification and scaling limits (74,75); (iii) rejection that is powerful but replaces bearing technology and adds substantial cost/complexity (76,77); and (iv) online active balancers proven in spindles but not yet adapted to the environmental and access constraints of utility-scale turbines (78,79). In contrast, the considered system is architected for continuous, trial-weight-free estimation under nonstationary wind operation and closed-loop, hub-integrated mass recentering, bridging the gap between diagnostic detection and true online mass correction while retaining compatibility with conventional drivetrains.

EXAMPLE OF POSSIBLE APPLICATION OF AN AUTOMATIC BALANCING SYSTEM IN WIND TURBINES

According to Niebsch and Ramlau (11), rotor imbalances can be categorized as mass and aerodynamic imbalances. Mass imbalances arise from inhomogeneous mass distributions of the rotor, including the blades and hub. Mass imbalances can be eliminated or reduced by balancing counterweights. Aerodynamic imbalances arise from deviations in the aerodynamic properties of blades. This leads to different thrust and tangential forces and moments, which depend not only on the rotational frequency but also on the wind speed. In addition to lateral vibrations, they induce axial and torsional vibrations in wind turbines. The main reason for the aerodynamic imbalance was the relative deviation of the blade pitch angles. This can be eliminated only by correcting these angles. Additional masses were not helpful. In practice, both types of imbalance are frequently observed, both separately and in combination. Wind turbines may sometimes have systems to correct the pitch angle to eliminate aerodynamic imbalance (14). Until now, there have been no such systems that could eliminate the mass imbalance in wind turbines during operation, and the aim was to eliminate this kind of unbalance. It was assumed that the pitch imbalance is corrected with the appropriate systems (80), and then only the mass imbalance is acted with.

Figure 14 presents the concept of using a balancing method with a continuous correction mass distribution applied to a wind turbine. The system was designed to measure the current vibration of a wind turbine bearing. The vibration caused by the imbalance caused by the mass of ice accumulated on a given turbine blade can be reduced by filling the opposite chambers with correction fluid. The arrangement of the chambers along the interior of the blade allows the volume of the chambers to be filled with fluid proportional to the given imbalance. Furthermore, controllable input and outlet valves allow continuous control of the amount of fluid accumulated in the hydroaccumulators, according to the scheme:

- inlet valve for the hydraulic tank (hydro accumulator),
- discharge valve for the hydraulic tank (hydro accumulator),
- hydraulic tank (hydro accumulator) inside the turbine blade,
- hydraulic channels with inlet/outlet valves and hydraulic tanks (hydro accumulators),
- rotary hydraulic connector supplying medium (liquid) to individual channels (turbine blades) from an external hydraulic system.

Placement of the balancing system inside the wind turbine blade

Amoretti et al. (81) showed the configurable dual-rotor wind turbine model based on the BEM method. Hijazi et al. (82) show a

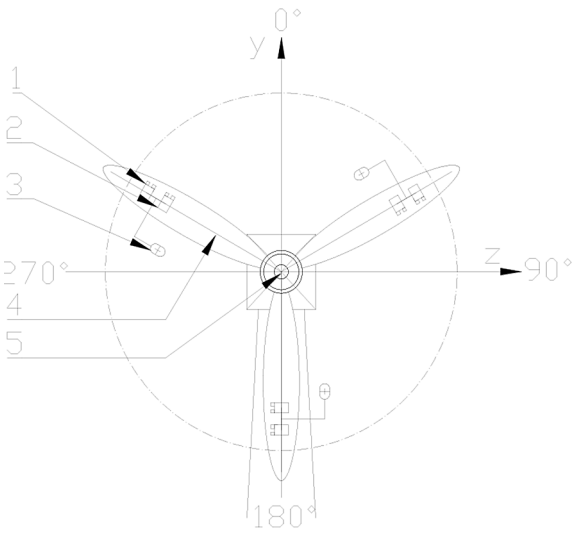

Figure 14. Schematic showing the feasibility of using a wind turbine balancing system with hydraulic tanks inside the blades for fluid to correct the unbalance caused by the ice layer mass

numerical investigation of the use of flexible blades for vertical-axis wind turbines. In each numerical model and practical application, there is space inside the rotor blade, and in this one compensation of mass could be added. Wang et al. [65] showed that an example of coupled aerostructural shape and topology optimization of horizontal axis wind turbine rotor blades was presented by Wang et al. (83) To regulate the position of the resulting correction mass, a wind turbine blade was proposed using hydraulic accumulators capable of storing single volumes of correction fluid. Figure 15 shows a cross section of a single wind turbine blade with the correction tanks in serial connection inside.

The geometry of the wind turbine blade allows the hydro accumulators to be arranged inside the wind turbine housing, assuming that various correction tanks will be used, such as Hydro Leduc's hydro accumulators. Placing a fluid tank near the tip of the wind turbine may be inappropriate. It can significantly alter the inertia of the blade, with adverse effects on the pitch actuators and blade fatigue. The location of such a tank must be optimized. There is a linear dependence between the imbalance force and the mass of the imbalance and its distance from the axis of rotation. The distance could be shortened twice and a double imbalance mass could be used, and the same value of the imbalance force would be obtained.

The largest tanks (ABVE50) will be located at a distance between 2 and 10 meters from the axis of rotation of the rotor, towards the tip of the blade. Then, at a distance between 11 and 31 meters, smaller tanks (ABVE32) will be placed, and the smallest tanks (ABVE20) will be placed at a distance between 32 and 42 meters. The distance between successive tanks will be 2 meters. With the tank scheme adopted, the maximum imbalance will be 17,900 kg·m, generating a centrifugal force of 28,238.53 N. A summary of the imbalance is given in Table 1. In the adopted simulations, the wind turbine rotates at a speed of 1.256 rad/s (approximately 12.1 rpm), resulting in centrifugal forces from the imbalance mass. A table with the locations of each type of correction tank (hydro accumulator) for the set speed is presented below. A Hydro Leduc, type ABVE, was suggested for the selection of the correction tank. A drawing of this hydro accumulator is shown in Figure 16.

NUMERICAL ANALYSIS OF THE IMBALANCE OF A WIND TURBINE

The Finite Element Method (FEM) is a powerful engineering tool that enables the solving of complex mechanical and structural problems by discretizing the area of analysis into smaller, more manageable elements. Specifically, in the realm of machine dynamics and rotor dynamics, FEM facilitates a detailed examination of the

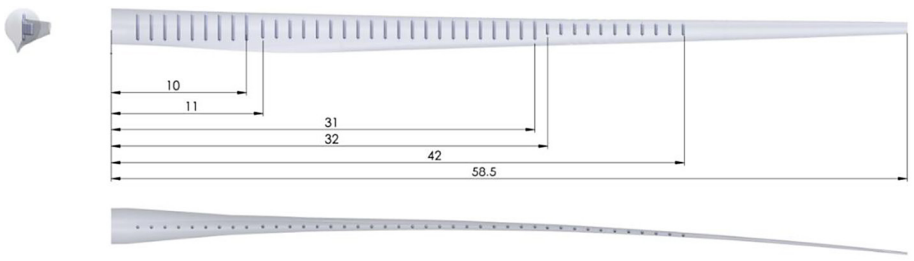

Figure 15. Cross section of a wind turbine blade with correction tanks

effects of imbalance, centrifugal forces, stresses, vibrations, and other factors that could impact the performance and stability of the system (85). The equation of motion is shown below:

$$\begin{matrix} \mathrm{M}\ddot{x}(t) + \mathrm{C}\dot{x}(t) + \\ +\mathrm{K}x(t) \ = \ \mathrm{F(t)} \end{matrix} \tag{7}$$

where: M denotes the system's mass matrix, C represents the damping matrix, K is the stiffness matrix, x symbolizes the displacement vector, $\dot{x}$ and $\ddot{x}$ are the first- and second-time derivatives of displacement, signifying velocity and acceleration, respectively, $F(t)$ is the vector of external forces acting on the system, dependent on time.

This equation reflects the dynamics of the system, taking into account the influence of mass, damping, and stiffness on the behavior of the rotors under various external forces. Solving this equation allows for the determination of displacements, velocities, and accelerations of rotor elements over time, which is crucial for understanding and predicting system behavior under load.

The force acting on the shaft is added by unbalance (86). The applied forces have sinusoidal character described by the following equation,

$$F_u = \mathrm{F}\cos\omega(\mathrm{t}) \tag{8}$$

The numerical solutions of the above differential equations include dynamic coefficients (87,88). The equations including these coefficients are presented below.

$$\begin{bmatrix} m_{xx} & m_{xy} \\ m_{yx} & m_{yy} \end{bmatrix} \ddot{x}(t) + \begin{bmatrix} c_{xx} & c_{xy} \\ c_{yx} & c_{yy} \end{bmatrix} \dot{x}(t) + \\ + \begin{bmatrix} k_{xx} & k_{xy} \\ k_{yx} & k_{yy} \end{bmatrix} x(t) = \begin{bmatrix} F_x(t) \\ F_y(t) \end{bmatrix}. \tag{9}$$

The analysis of wind turbine rotor imbalance requires precise understanding and modeling of rotor dynamics, where FEM plays a pivotal role. Rotor imbalance can lead to undesirable vibrations, increasing the risk of machine damage or even failure. Utilizing the equation of motion within the FEM context allows for a detailed analysis of the system's response to imbalance, facilitating the identification of potential issues and the development of mitigation strategies.

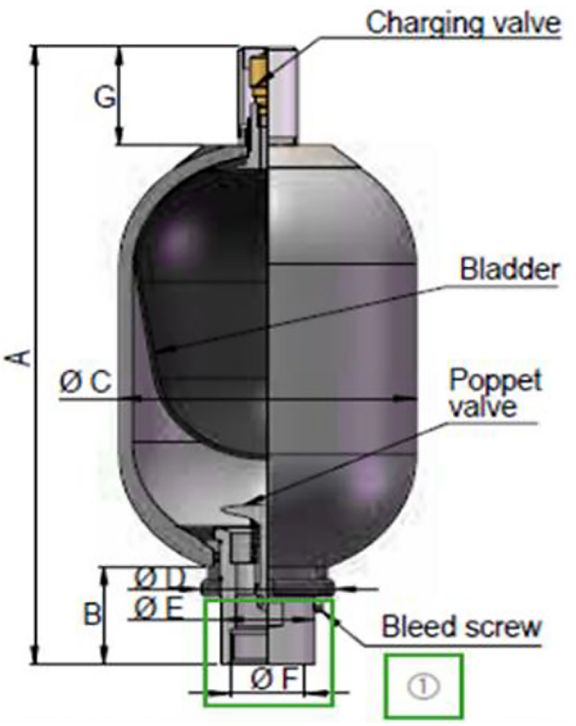

Figure 16. Correction tank

The integration of theoretical FEM principles and the differential equation of motion serves as a foundation for further discussions on the specifics of analyzing wind turbine rotor imbalance. Understanding these fundamental concepts is essential to fully grasping the complexity of the problem and the methods used for its resolution, which will be elaborated on in subsequent sections of the article.

This chapter shows an example of a numerical analysis that confirms the feasibility of the concept of a unique, patented, automatic balancing system first applied to wind turbines. To test the applicability of the method, a new numerical model was needed. The article was focused on the rotor-dynamic performance of a wind turbine

Table 1. Hydroaccumulator dimensions (84)

ABVE	Nitrogen capacity Vo (liters)			Max. pressure (bar)		Mass (kg)	Dimensions (mm)			
				A	B	ØC	ØD	ØE	ØF	G
ABVE 20	17.6	330	45	878.4	102	223	101	76	G2”	65.4
ABVE 32	32.7	330	80	1,403.4	102	223	101	76	G2”	65.4
ABVE 50	48.9	330	110	1,926	102	223	101	76	G2”	73

with a power of about 5 MW. Some analyses can be found in a paper describing the design of a 6 MW turbine (89), but the analysis presented in the paper is mainly focused on the blade of this wind turbine. Kusnick et al. (90) also provided information on this issue, but focused on the nacelle and blade measurements. This paper bridges that gap by showing how an automatic balancing system for wind turbines can improve their safety. This is the first attempt reported in the literature to implement this system for wind turbines.

To model the effect of the automatic balancing system on the wind turbine, a beam model was created in Madyn 2000 software. The shaft geometry corresponds to that of a 5 MW offshore turbine and was modeled after the report by Jonkman et al. (11). Figure 17 shows a schematic drawing of a wind turbine with basic dimensions.

Description of the numerical model

The nominal speed of the wind turbine is 12.1 rpm. The rotor shaft was modeled using 60 beam elements. The rotor blades were modeled as additional sections located above the beam elements from number 5 to number 14. Steel with a density of 7.860 kg/m^3 was assumed as the entire shaft. The wind blades were modeled using a disc (with steel parameters), the density of which was reduced to provide the same mass as the three rotor blades. The shaft was based on junctions 29 and 49. The 3D model of the wind turbine along with the coordinate system is shown in Figure 18 (a). Part (b) presents a close-up of the central portion of the rotor with the bearings marked. The blue color indicates the blades of the wind turbine. The working principle of automatic balancing was analyzed. The system aimed to minimize lateral vibration. The torsional and axial vibrations were not analyzed because they usually do not have a direct impact on lateral vibrations. During the numerical calculations, stable wind conditions were assumed, and because of that, during the operations, there was no need to act as the controller.

The shaft of the wind turbine is inclined to the horizontal axis by 5 degrees, which was realized in the numerical model by appropriately dividing the gravitational force; 95% of its value was directed perpendicularly to the rotor axis (y direction), while 5% of its value in the perpendicular direction (x direction).

The design retains the same overall dimensions as those of the offshore 5 MW wind turbine. The distance between the hub and the first bearing is 1.900 mm and the distance between the bearings is 2.000 mm. The weight of the hub is 56,800 kg and the mass of the blades is 17,700 kg. Including the shaft, the total weight of the rotor is 110,000 kg. The total length of the rotor was 6 m, while the diameter of its blades was 126 m. In practice, the shafts of wind turbines on which the blades are located are connected to the power generator using the appropriate gears. The most common type of gearbox is a two-stage planetary gear combined with a helical gear. This arrangement allows the speed to increase from 12.1 rpm to 1,173.7 rpm with a 97:1 gear ratio (92). As part of the dynamic analyses performed, only the first rotor, including the blades, was included in the model. The part related to the gearbox and generator was not included because it only slightly affects the lateral vibration and imbalance of

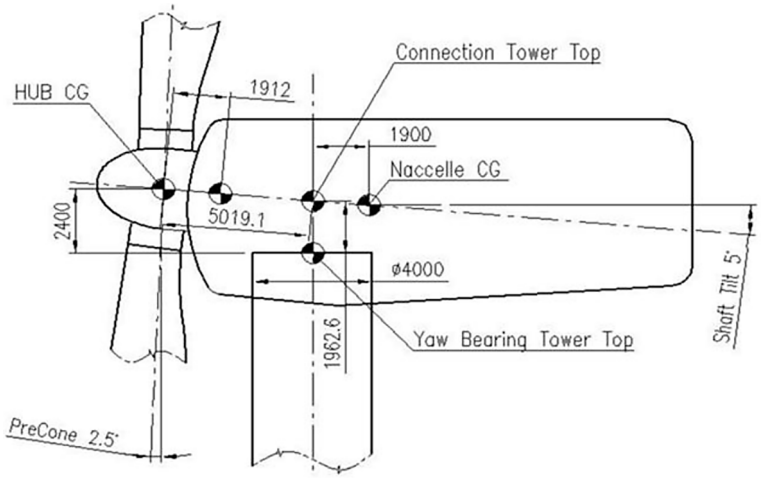

Figure 17. Schematic of a 5 MW offshore wind turbine according to (91)

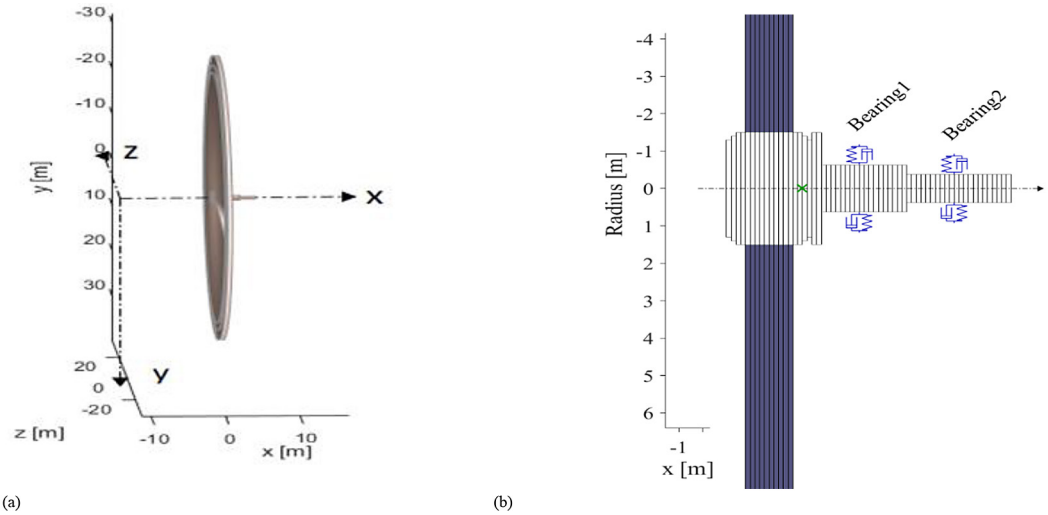

Figure 18. (a) 3D model of the wind turbine, including the coordinate system; (b) view of the shaft, including bearings

the turbine blades, and this was the main focus of the analysis. The calculation model used does not allow for including aeroelastic forces coming from the blades of the wind turbine.

There are many possible bearing arrangements for offshore wind turbines, as presented by Torsvik et al. (93). The authors presented development trends and design requirements. The bearing parameters were adopted from the publication of Nejad et al. (35). The first bearing was a CARB (Compact Aligning Roller Bearing) type bearing with an outer diameter of 1.750 mm, an inner diameter of 1.250 mm, and a width of 375 mm. The second type of SRB bearing (spherical roller bearing) has an outer diameter of 1,220 mm, an inner diameter of 750 mm, and a width of 365 mm. A summary of the parameters is given in Table 2.

Bearing stiffness can be defined according to Equation 3:

$$K = [k_x 00000 k_y 0000 k_z 000 k_\alpha 00\text{sym}.k_\beta 0 k_\gamma]$$

The stiffness coefficients were adopted based on the publications of Nejad et al. (35). The damping coefficients were adopted based on the data presented by Zeillinger (94). A summary of these data is presented in Table 3.

The main forces that act on a wind turbine come from airflow. The load can be assumed to be equal to the values reported by Guo et al. (95), which are summarized in Table 4. Lindenburg et al. (89) was 3.42 MN·m. It is numerically important to determine the effect of support (96). This happens because the frequency of rotation is different from the frequency at which the floating platform moves. To show how the imbalance affects the wind turbine, the support was treated as rigid.

Imbalance cases analyzed

Inequality may occur due to poor manufacturing; however, before commissioning a turbine, technicians generally rebalance the rotor by adding compensating masses to achieve a residual imbalance (G16) that is considered safe for operation (90) System imbalances can come from different

Table 2. Properties of the NREL offshore 5-MW baseline wind turbine

Items	Unit	Specification
Rotor, hub diameter	M	126.3
Cut-in, rated, cut-out wind speed	m/s	3, 11.4, 25
Cut-in, rated rotor speed	rpm	6.9, 12.1
Overhang, shaft tilt, precise	m, deg, deg	5, 5, 2.5
Rotor mass	kg	110,000
Nacelle mass	kg	240,000
Nacelle size (length, width, height)	m	19, 6, 7

Table 3. Damping stiffness coefficient values

Fx [kN]	Fy [kN]	Fz [kN]	Mx [kNm]	My [kNm]	Mz [kNm]
255	-180	-1.300	5.000	-14,000	-5.500

sources, for example, aeroelastic phenomena, mechanical problems, and icing. In the article, the authors did not distinguish between these phenomena, but the calculation cases that include the worst-case scenario were used for the calculation (the highest imbalance), because under these conditions balancing would be the most demanding. The presence of aerodynamic imbalances in addition to mass imbalances would lead to additional lateral forces, but the authors assumed in this model that aerodynamic imbalances were not present. The paper analyzed three computational cases with different imbalance values. The first case assumed an imbalance of 1.400 kg·m. It is based on the ISO 1940-1 standard (58) for G16 balance grade G16 and has a rotor speed of 12.1 rpm. Table 5 shows a summary of the imbalance values for the three cases 5. A graphical representation of the imbalance is shown in Figure 19. There are a couple of ways to fill the tanks. The hydraulic swivel joint could be used. In this scenario, the fluid that will be used to fill the container may be stored in the wind turbine tower.

In the second case of imbalance analyzed, it was assumed that the wind turbine blade was icy during operation. According to the literature, the imbalance of an iced blade of a 5 MW wind turbine can be assumed to be 21,000 kg·m. The calculation assumes the most dangerous case from a dynamic point of view, i.e. the sum of the imbalance due to ice and the maximum allowable imbalance. Therefore, the total imbalance was 22,400 kg·m.

In the third calculation case, the operation of the automatic balance system was considered. An imbalance of 22,400 kg·m was left on one of the blades. Balancing masses of 15,000 kg·m each were added to the other two blades placed at 120° and 240°. The total imbalance was thus 7.400 kg·m, a value almost three times smaller than the earlier value taken in the second case of calculation.

Table 4. Wind turbine load values are based on (95)

Bearing	k_x [N/m]	k_y [N/m]	k_z [N/m]
Bearing No. 1	0	$1.5 \cdot 10^{10}$	$1.5 \cdot 10^{10}$
Bearing No. 2	$4.06 \cdot 10^{8}$	$1.54 \cdot 10^{10}$	$1.54 \cdot 10^{10}$
	k_β [rad/s]	k_γ [rad/s]	
Bearing No. 1	$5 \cdot 10^{6}$	$5 \cdot 10^{6}$	
Bearing No. 2	0	0	
	c_y [N·s/m]	c_z [N·s/m]	
Bearing No. 1	1.000	1.000	
Bearing No. 2	1.000	1.000	

Analysis with maximum permissible imbalance (Case I)

The research included calculations for the maximum allowable imbalance according to grade G16, which is 1.400 kg·m. The results can be found in Figures 21–27. Figure 20 presents the first two forms of natural vibration, which occurred at 6.61 and 59.85 Hz. After comparing these values with a rotational speed of 12.1 rpm or 0.202 Hz, it was found that in the nominal speed range and during the upwind, the wind turbine is not affected by resonant vibrations of the entire rotor.

Figure 21 shows the displacements (a) as well as the forces and moments acting on the wind turbine shaft. There are no experimental data in the literature for the operation of a 5-MW wind turbine with which the results obtained can be directly obtained. The results obtained for the three calculation cases analyzed can be compared with each other to obtain a picture of how different values and imbalance configurations affect the dynamic properties of the wind turbine. In the case analyzed, the peak-to-peak displacement values were approximately 4 µm, the maximum forces in the bearings were approximately 3.000 N, and the bending moments were approximately 4.000 N·m. The reduced stresses were small and did not exceed 0.1 MPa (Figure 22). The trajectories at the central part of the hub, i.e., at node 10 are shown in Figure 23. The figure shows that the diameter of this trajectory was less than 3 µm.

Analysis of the imbalance caused by an iced wind turbine blade (Case II)

An imbalance of 22,400 kg·m was assumed for the numerical calculations. This is a summation that considers the value of the maximum allowable imbalance (according to the balance

Table 5. Summary of imbalance cases

Case No.	Blade No.	Angle [°]	Imbalance value [kg·m]
Case I	1	0	1.400
	2	120	0
	3	240	0
Case II	1	0	22,400
	2	120	0
	3	240	0
Case III	1	0	22,400
	2	120	15,000
	3	240	15,000

grade G16) and the imbalance of the wind turbine blade due to ice. The results of displacements and bending forces and moments are shown in Figure 24. The peak-to-peak displacements were approximately 45 µm. The maximum forces were about 50,000 N while the moments were about 50,000 N/m. The trajectories showing the displacements of the hub at an unweighting increased by fifteen times compared to the first calculation case are shown in Figure 25. It can be seen that the vibration has increased from 3 µm to about 45 µm.

Analysis after balancing process (Case III)

In the third calculation case, the imbalance modeled earlier for one blade of the wind turbine was also applied to the second blade (at node 11) and the third (at node 9) of the turbine. Therefore, the total imbalance was 21,000 kg·m, 15,000 kg·m, and 15,000 kg·m. The total residual imbalance was 7.400 kg·m. There was an angle of 120 degrees between the imbalances. The displacement values are summarized in Figure 26 (a), while the force and moment values are shown in Figure 26 (b). The trajectories for the hub are shown in Figure 27. The peak-to-peak displacement value for node 10 was approximately 15 µm.

The results for the second and third calculation cases are very close to each other. This is because the two imbalances operate at different angles. Since the imbalance should be treated as a vector, therefore, its real effect on the structures despite the doubling of the imbalance did not result in double displacement values.

MECHANICAL FATIGUE

Mechanical fatigue in wind turbines is mainly due to material degradation under cyclic loading. In the case of wind turbines, which are exposed to regular load changes during operation, mechanical fatigue results in a loss of structural life of components such as shafts, bearings, or blades (97,98). During the initial life of a wind turbine, structures and components subjected to cyclic loads may be subjected to microcracks and microdamage. They may not be visible to the naked eye, but represent the beginning of the fatigue process. Over time, cracks can grow, and this process can be accelerated by imbalance, adverse

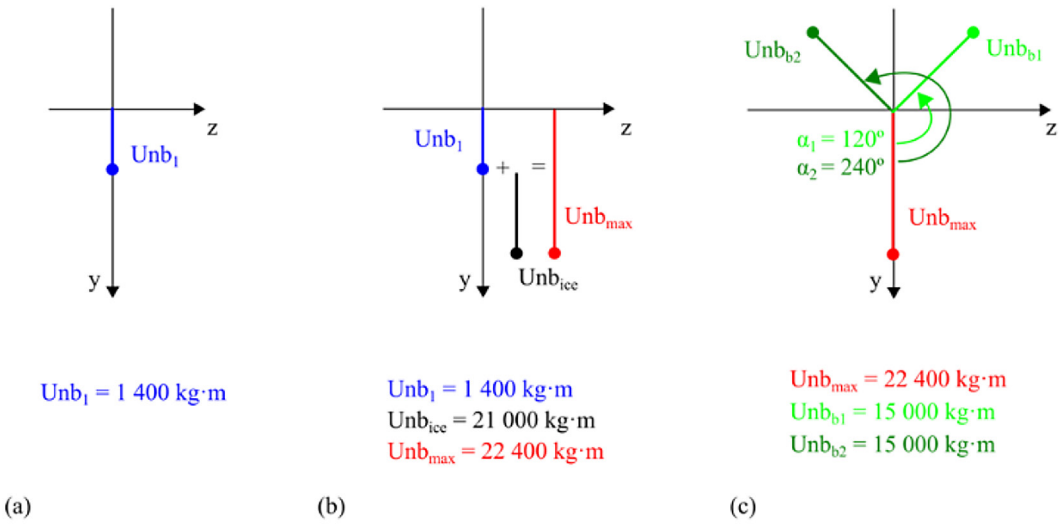

Figure 19. Graphical representation of the imbalance for the three cass analyzed: (a) ISO 1940 grade G16 permissible imbalance – 1.400 kg·m, (b) a summed imbalance of the ice blade and residual imbalance – 22,400 kg·m, (c) imbalance after the balance system tripped – 7.400 kg·m

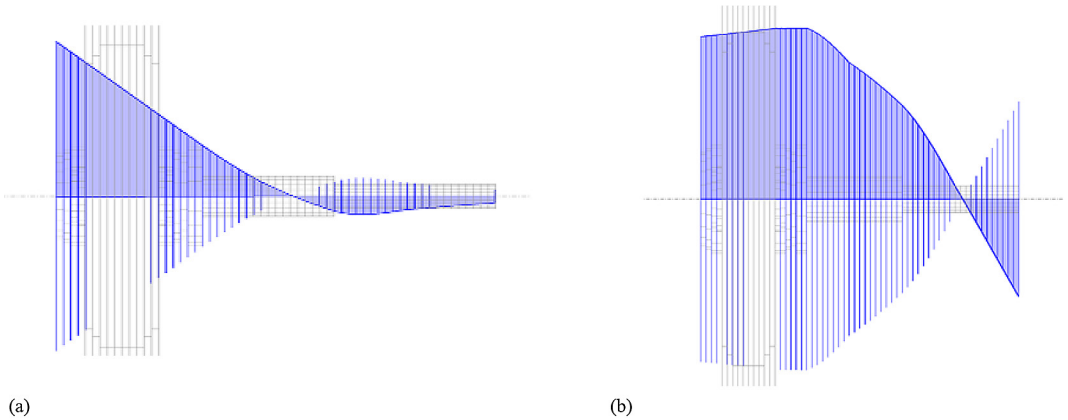

Figure 20. The first two forms of transverse vibration for frequencies: 4.26 Hz (a) and 57.88 Hz (b)

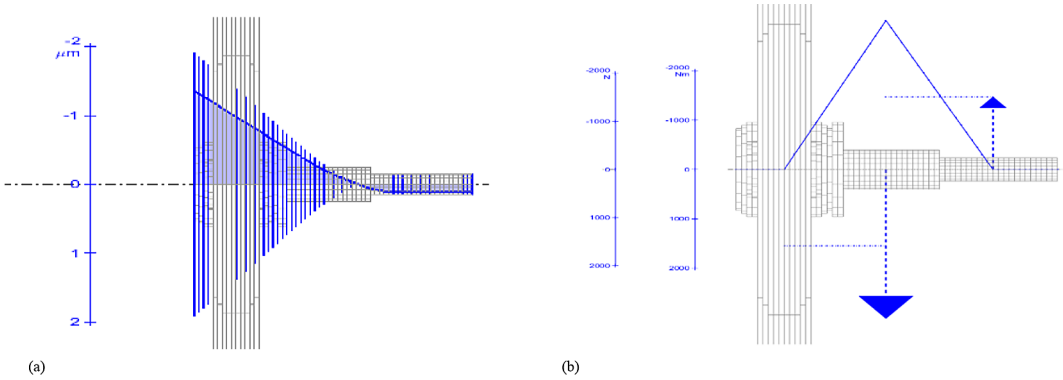

Figure 21. (a) Displacements at an imbalance of 1.400 kg·m, (b) forces and moments

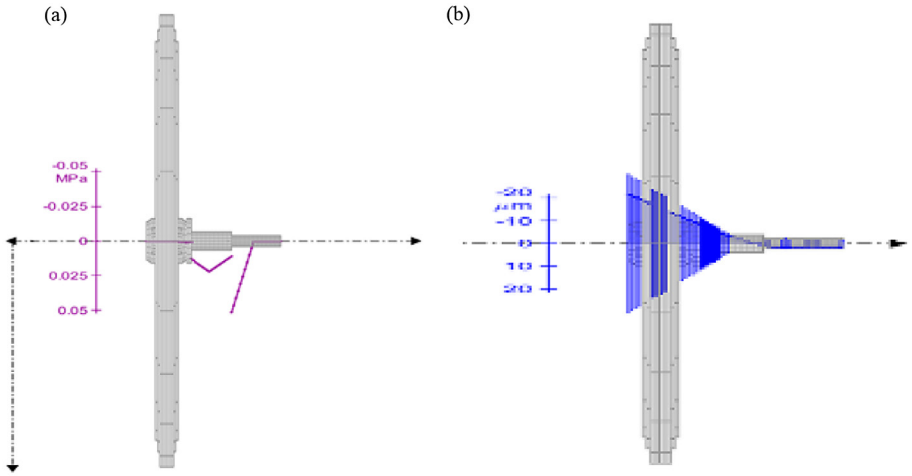

Figure 22. Reduced stresses

weather conditions, and changes in direction and force. This phenomenon leads to increased stresses and accelerates the process of structural degradation. Mechanical fatigue leads to structural failure or component failure. These may include not only blade fractures, but also bearing damage or shaft deformation. This requires replacement of the damaged parts or even entire turbines. It is necessary to monitor the technical condition of wind turbines as well as perform regular maintenance and inspections. These include tracking rotor imbalance, aerodynamic asymmetry, surface roughness, and overall performance, as well as stress and strain measurements (99). Without

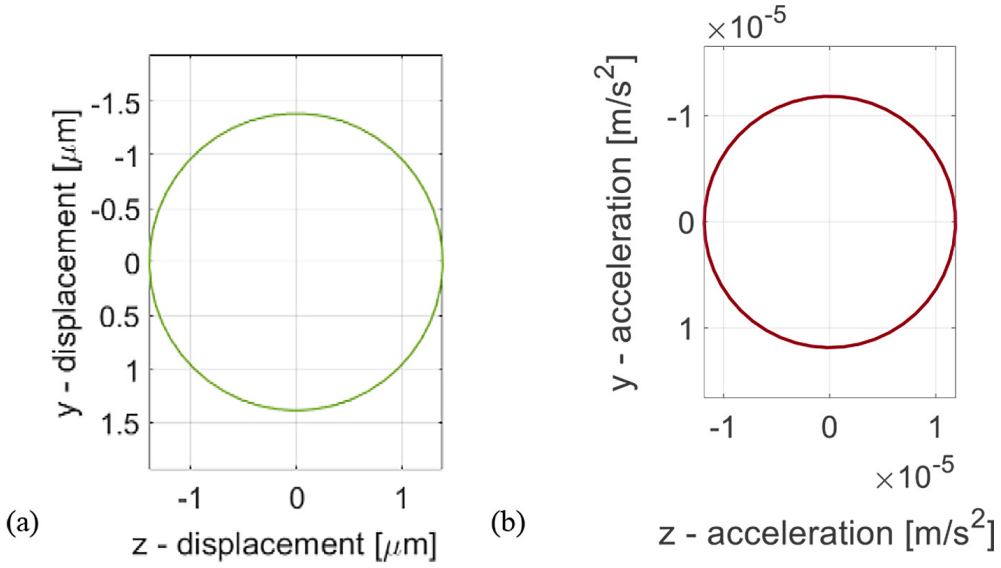

Figure 23. Trajectory: a) displacements, b) accelerations of the hub with an imbalance of 1.400 kg·m

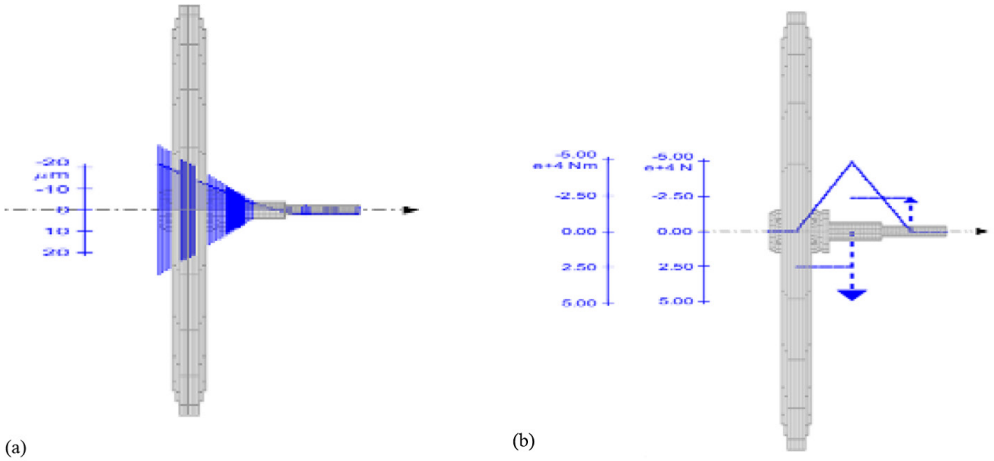

Figure 24. (a) Displacements in an imbalance of 22,400 kg·m, (b) forces and moments

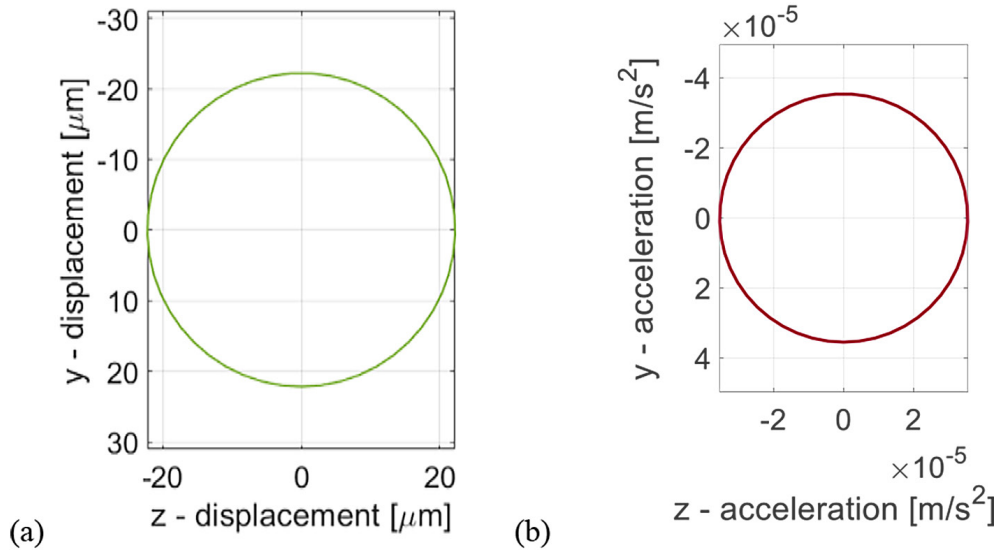

Figure 25. Trajectory: (a) displacements, (b) accelerations of the hub with an imbalance of 22,400 kg·m

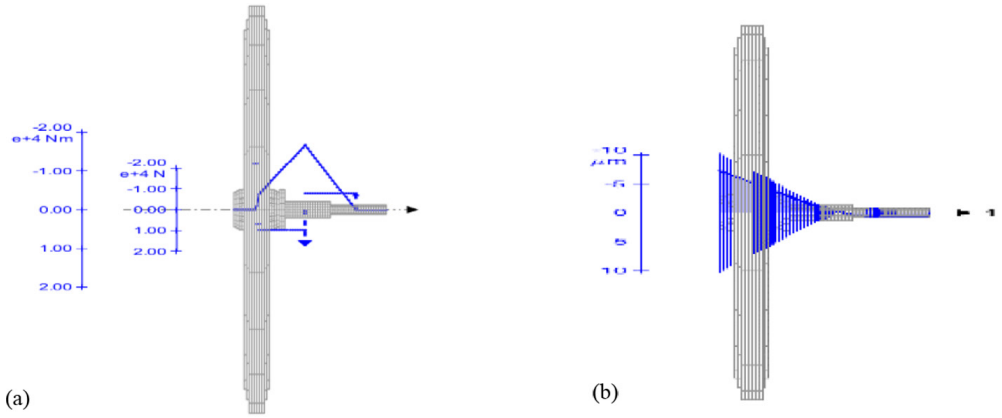

Figure 26. (a) Displacements in an imbalance of 7.400 kg·m, (b) forces and moments

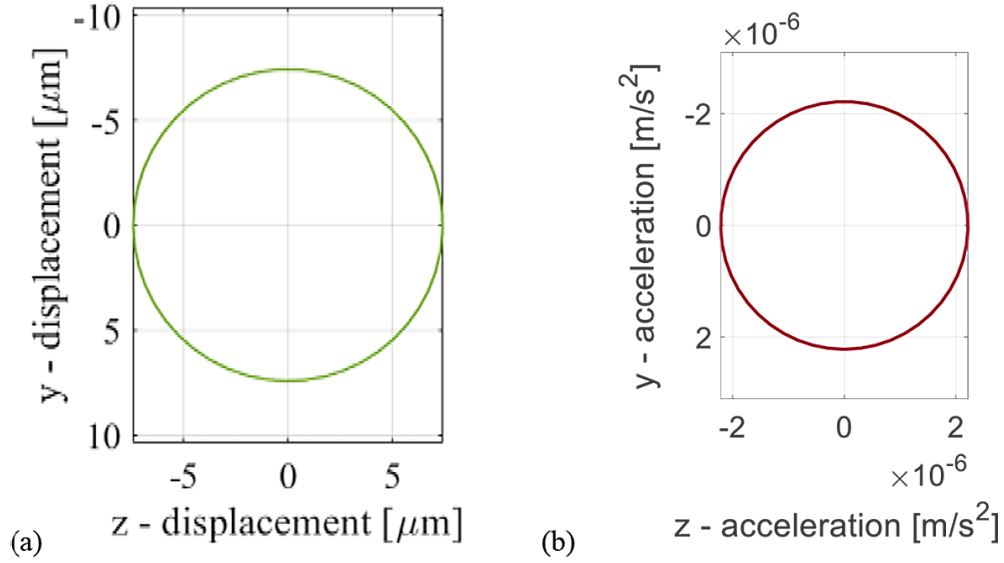

Figure 27. Trajectory: a) displacements, b) accelerations of the hub, with an imbalance of 7.00 kg·m

implementing such measures, potential problems can go unnoticed, leading to the possibility of more severe damage resulting from mechanical fatigue processes. Fatigue damage for the designed service life of the turbine is evaluated using the Goodman diagram and the S-N curve (stress vs. number of cycles).

The design life of the main shaft bearing is 20 years. In the prediction of paper (100) the fatigue life of a main shaft bearing was investigated: 240/630CA/W33 double row self-aligning roller bearing. The S-N curve of the main shaft bearing is expressed by Equation 1:

$$N = CS^{-\alpha} = C\left\{\frac{q(K_T - 1) + 1}{\varepsilon\beta C_t} S_{-1}\right\}^{-\alpha} \quad (10)$$

where: N is the fatigue life; C and α are material constants; S is the maximum stress or the stress amplitude under a certain stress ratio; q is the notch sensitivity factor; K_T is the theoretical stress concentration factor; ε is the size factor; β is the surface quality factor; CL is the loading method, $S\text{-}1$ is the stress amplitude of the component.

The fatigue life of the main shaft bearing (t) is calculated by Equation 2:

$$t = \frac{N}{365 \times 24 \times 60n} \quad (11)$$

On the basis of the results of contact stress analysis, according to the nominal stress approach and the cumulative fatigue damage rule, the fatigue life of a wind turbine can be predicted.

The bearing of the main shaft is 24.07 years under the combined action of different working

conditions. The prediction result complies with the requirement of the 20-year design life of a wind turbine. Mechanical parameters required for fatigue analysis, such as load cycles, maximum stress, minimum stress, mean stress, stress amplitude, and equivalent stress, are obtained from the sample spectrum data collected during short-term operation (101). The wind-induced load that fluctuates in real time is irregular and stochastic, and the corresponding load history intricately influences the fatigue life of the components.

CONCLUSIONS

This article discussed a new method that can improve the safety and efficiency of wind turbines by automatically balancing them. The solution involves using a correction fluid to address any imbalances in the blades that may arise from factors such as ice accumulation. Correction elements are inserted within the turbine blades, and an automatic balancing system prolongs the turbine's service life while boosting its safety. The article also provides information on the balance of the rotor and how imbalances can lead to fatigue loading, ultimately resulting in blade breakage. By implementing this proposed solution, wind turbines can operate more efficiently, reducing downtime and maintenance costs resulting from imbalances.

In this paper, a 3D model and an analysis of a 5 MW offshore wind turbine were carried out, considering rigid support and bearing stiffness. The study examined the effects of varying the imbalance values on the vibrations generated by the wind turbine. It was discovered that an automatic wind turbine balancing system could be implemented for wind turbines and that blade icing could cause an imbalance that exceeds the ISO 1940-1 standard. After the balancing process, the vibration level dropped to an acceptable value according to the same standard. The simulations confirmed that an automatic wind turbine balancing system could be implemented for wind turbines.

The fatigue analysis performed shed light on the degradation processes of wind turbine components under cyclic loads, offering perspectives on increasing the durability of turbines through optimization of the balancing processes. The fatigue analysis also highlighted the importance of precise balance to prevent fatigue damage, which can significantly affect the long-term performance and safety of wind turbines.

Rotor imbalances can be classified into mass and aerodynamic imbalances. Mass imbalances arise from the uneven distribution of the rotor's mass, while aerodynamic imbalances are caused by deviations in the aerodynamic properties of the blades. Both types of imbalances can cause vibrations in wind turbines, but aerodynamic imbalances can also induce axial and torsional vibrations. The possibility of minimizing aerodynamic imbalance using an automatic balancing system is an area for future research. The main cause of aerodynamic imbalance is the relative deviation of the blade pitch angles, which can be corrected by adjusting these angles. Additional masses are not helpful in this case. To eliminate mass imbalance, an automatic balance system is needed, independent of other wind turbine systems. The system is triggered by unbalance in the system, such as ice on the blade, as well as decreases vibration levels, improving the dynamic properties of the rotor and extending the lifetime of the drivetrain.

Implementing effective condition monitoring and maintenance strategies is essential to optimize wind turbine performance and service life, thus supporting sustainable energy generation. Evolving policies and regulations help to maintain sustainable decommissioning of wind turbines, ensuring alignment with broader environmental goals. By integrating sustainable practices throughout the life cycle of the turbine, the wind energy sector enhances its role in combating climate change and promoting environmental stewardship. This approach ensures that wind energy remains a sustainable and responsible option for the future, and increasing the reliability of the turbine aligns with the principles of the circular economy, promoting efficient use and waste reduction.

Acknowledgments

This paper was created within the framework of the ACTIVERING project entitled "Aktywne łożyska foliowe ze zmiennymi właściwościami dynamicznymi" (Eng. Active foil bearings with variable dynamic properties), agreement no. LIDER/51/0200/L9/17/NCBR/2018, implemented as part of the research and development program called "LIDER" (Eng. LEADER). Calculations were carried out at the Academic Computer

Center in Gdansk. Research project supported/ partly supported by program "Excellence initiative - research university" for the AGH University of Krakow.

REFERENCES

1. Blanco MI. The economics of wind energy. Renew Sustain Energy Rev. 2009;13(6–7):1372–82.
2. Tremeac B, Meunier F. Life cycle analysis of 4.5 MW and 250 W wind turbines. Renew Sustain Energy Rev. 2009;13(8):2104–10.
3. Martínez E, Sanz F, Pellegrini S, Jiménez E, Blanco J. Life cycle assessment of a multi-megawatt wind turbine. Renew Energy. 2009;34(3):667–73.
4. Bank LC, Arias FR, Yazdanbakhsh A, Gentry TR, Al-Haddad T, Chen JF, et al. Concepts for reusing composite materials from decommissioned wind turbine blades in affordable housing. Recycling. 2018;3(1).
5. Fingersh L, Hand M, Laxson A. Wind turbine design cost and scaling model [Internet]. Golden, CO; 2006 Dec. Available from: http://www.osti.gov/servlets/purl/897434-Feoadi/
6. Chou JS, Chiu CK, Huang IK, Chi KN. Failure analysis of wind turbine blade under critical wind loads. Eng Fail Anal [Internet]. 2013;27:99–118. Available from: http://dx.doi.org/10.1016/j.engfailanal.2012.08.002
7. Ramlau R, Niebsch J. Imbalance estimation without test masses for wind turbines. J Sol Energy Eng [Internet]. 2009 Feb 1;131(1):0110101–7. Available from: https://asmedigitalcollection.asme.org/solarenergyengineering/article/doi/10.1115/1.3028042/444127/Imbalance-Estimation-Without-Test-Masses-for-Wind
8. Im H, Kim B. Numerical study on the effect of blade surface deterioration by erosion on the performance of a large wind turbine. J Renew Sustain Energy. 2019;11(6).
9. Saathoff M, Rosemeier M, Kleinselbeck T, Rathmann B. Effect of individual blade pitch angle misalignment on the remaining useful life of wind turbines. Wind Energy Sci. 2021;6(5):1079–87.
10. Frohboese P, Anders A. Effects of icing on wind turbine fatigue loads. J Phys Conf Ser. 2007;75(1).
11. Niebsch J, Ramlau R. Simultaneous estimation of mass and aerodynamic rotor imbalances for wind turbines. J Math Ind. 2014;4(1):1–19.
12. Breńkacz Ł, Żywica G, Bogulicz M. Selection of the oil-free bearing system for a 30 kW ORC microturbine. J Vibroengineering [Internet]. 2019 Mar 31;21(2):318–30. Available from: https://www.jvejournals.com/article/19980/pdf
13. Breńkacz Ł, Żywica G, Bogulicz M. Selection of the Bearing System for a 1 kW ORC Microturbine. In: Mechanisms and Machine Science [Internet]. 2019;223–35. Available from: http://link.springer.com/10.1007/978-3-319-99262-4_16
14. Cacciola S, Riboldi CED, Croce A. Monitoring rotor aerodynamic and mass imbalances through a self-balancing control. J Phys Conf Ser. 2018;1037(3).
15. Colín Ocampo J, Gutiérrez Wing ES, Ramírez Moroyoqui FJ, Abúndez Pliego A, Blanco Ortega A, Mayén J. A novel methodology for the angular position identification of the unbalance force on asymmetric rotors by response polar plot analysis. Mech Syst Signal Process. 2017 Oct 1;95:172–86.
16. Choudhury T, Viitala R, Kurvinen E, Viitala R, Sopanen J. Unbalance estimation for a large flexible rotor using force and displacement minimization. Machines. 2020 Sep 1;8(3).
17. Hübner GR, Pinheiro H, de Souza CE, Franchi CM, da Rosa LD, Dias JP. Detection of mass imbalance in the rotor of wind turbines using Support Vector Machine. Renew Energy [Internet]. 2021;170:49–59. Available from: https://doi.org/10.1016/j.renene.2021.01.080
18. Freeman B, Tang Y, Huang Y, VanZwieten J. Rotor blade imbalance fault detection for variable-speed marine current turbines via generator power signal analysis. Ocean Eng. 2021 Mar 1;223.
19. Breńkacz Ł, Żywica G, Drosińska-Komor M, Szewczuk-Krypa N. The Experimental Determination of Bearings Dynamic Coefficients in a Wide Range of Rotational Speeds, Taking into Account the Resonance and Hydrodynamic Instability. In: Springer Proceedings in Mathematics and Statistics [Internet]. 2018. Available from: http://www.scopus.com/inward/record.url?eid=2-s2.0-85053848493&partnerID=MN8TOARS
20. Caselitz P, Giebhardt J. Rotor condition monitoring for improved operational safety of offshore wind energy converters. J Sol Energy Eng Trans ASME. 2005;127(2):253–61.
21. Hameed Z, Hong YS, Cho YM, Ahn SH, Song CK. Condition monitoring and fault detection of wind turbines and related algorithms: A review. Renew Sustain Energy Rev. 2009;13(1):1–39.
22. Xiaoxun Z, Xinyu H, Xiaoxia G, Xing Y, Zixu X, Yu W, et al. Research on crack detection method of wind turbine blade based on a deep learning method. Appl Energy. 2022;328(October).
23. Niebsch J, Ramlau R, Nguyen TT. Mass and Aerodynamic Imbalance Estimates of Wind Turbines. Energies [Internet]. 2010 Apr 8;3(4):696–710. Available from: http://www.mdpi.com/1996-1073/3/4/696
24. Xing Z, Chen M, Cui J, Chen Z, Xu J. Detection of magnitude and position of rotor

aerodynamic imbalance of wind turbines using Convolutional Neural Network. Renew Energy. 2022 Sep;197:1020–33.

25. Kral C, Habetler TG, Harley RG. Detection of mechanical imbalances of induction machines without spectral analysis of time-domain signals. IEEE Trans Ind Appl. 2004 Jul;40(4):1101–6.
26. Xu J, Ding X, Gong Y, Wu N, Yan H. Rotor imbalance detection and quantification in wind turbines via vibration analysis. Wind Eng [Internet]. 2022 Feb 17;46(1):3–11. Available from: http://journals.sagepub.com/doi/10.1177/0309524X21999841
27. Blaut J, Breńkacz Ł. Application of the teager-kaiser energy operator in diagnostics of a hydrodynamic bearing. Eksploat i Niezawodn. 2020;22(4):757–65.
28. Johnson SJ, Larwood S, McNerney G, Dam CP. Balancing fatigue damage and turbine performance through innovative pitch control algorithm. Wind Energy [Internet]. 2012 Jul;15(5):665–77. Available from: https://onlinelibrary.wiley.com/doi/10.1002/we.495
29. Łosiewicz Z, Mironiuk W, Cioch W, Sendek-Matysiak E, Homik W. Application of generator-electric motor system for emergency propulsion of a vessel in the event of loss of the full serviceability of the diesel main engine. Energies [Internet]. 2022 Apr 13;15(8):2833. Available from: https://www.mdpi.com/1996-1073/15/8/2833
30. Pawlik P. Single-number statistical parameters in the assessment of the technical condition of machines operating under variable load. Eksploat i Niezawodn. 2019;21(1):164–9.
31. Blaut J, Breńkacz Ł. Application of the dispersion entropy with sliding window for the analysis of mechanical systems. Diagnostyka [Internet]. 2024 Nov 12;25(4):1–12. Available from: http://www.diagnostyka.net.pl/Application-of-the-dispersion-entropy-with-sliding-window-for-the-analysis-of-mechanical,195473,0,2.html
32. Blaut J. Application of dispersion entropy to journal bearing hydrodynamic stability. Vib Phys Syst [Internet]. 2024;35(2). Available from: https://vibsys.put.poznan.pl/_journal/2024-35-2/articles/vps_2024217.pdf
33. Wróbel J, Blaut J. Influence of pressure inside a hydraulic Line on its natural frequencies and mode shapes. In 2021. p. 333–43. Available from: http://link.springer.com/10.1007/978-3-030-59509-8_30
34. Hofmann M, Sperstad IB. Will 10 MW wind turbines bring down the operation and maintenance cost of offshore wind farms? Energy Procedia [Internet]. 2014;53(C):231–8. Available from: http://dx.doi.org/10.1016/j.egypro.2014.07.232
35. Nejad AR, Guo Y, Gao Z, Moan T. Development of a 5 MW reference gearbox for offshore wind turbines. Wind Energy [Internet]. 2016 Jun;19(6):1089–106. Available from: https://onlinelibrary.wiley.com/doi/10.1002/we.1884
36. Xu K, Meng A, Chang S, Liu D, Liu F. Synergy of random balance design method and intelligent optimization technique for model updating of the 4 MW offshore wind turbine benchmark. Mar Struct [Internet]. 2024;93(October 2023):103533. Available from: https://doi.org/10.1016/j.marstruc.2023.103533
37. Ren Z, Verma AS, Li Y, Teuwen JJE, Jiang Z. Offshore wind turbine operations and maintenance: A state-of-the-art review. Renew Sustain Energy Rev. 2021;144(February).
38. Sovacool BK, Enevoldsen P, Koch C, Barthelmie RJ. Cost performance and risk in the construction of offshore and onshore wind farms. Wind Energy [Internet]. 2017 May 14;20(5):891–908. Available from: https://onlinelibrary.wiley.com/doi/10.1002/we.2069
39. Miaskowski W, Nalepa K, Pietkiewicz P, Piechocki J. Small-scale wind power energy systems for use in agriculture and similar applications. In: Bundschuh J, Chen G, Chandrasekharam D, Piechocki J, editors. Geothermal, Wind and Solar Energy Applications in Agriculture and Aquaculture. 2017; 259–88. (Sustainable Energy Developments; vol. 13).
40. Čepin M. Evaluation of the power system reliability if a nuclear power plant is replaced with wind power plants. Reliab Eng Syst Saf. 2019;185(August 2018):455–64.
41. Li H, Guedes Soares C, Huang HZ. Reliability analysis of a floating offshore wind turbine using Bayesian Networks. Ocean Eng. 2020;217(September).
42. Darlow MS. Balancing of High-Speed Machinery [Internet]. New York, NY: Springer New York; 1989; 196. (Mechanical Engineering Series). Available from: http://link.springer.com/10.1007/978-1-4612-3656-6
43. Łączkowski R. Wyważanie elementów wirujących [eng: Balancing of rotating components]. 1st ed. Warszawa: Wydawnictwa Naukowo-Techniczne; 1979.
44. Al-Shudeifat MA, Butcher EA, Stern CR. General harmonic balance solution of a cracked rotor-bearing-disk system for harmonic and sub-harmonic analysis: Analytical and experimental approach. Int J Eng Sci [Internet]. 2010;48(10):921–35. Available from: http://dx.doi.org/10.1016/j.ijengsci.2010.05.012
45. Breńkacz Ł, Witanowski Ł, Drosińska-Komor M, Szewczuk-Krypa N. Research and applications of active bearings: A state-of-the-art review. Mech Syst Signal Process [Internet]. 2021 Apr;151:107423. Available from: https://linkinghub.elsevier.com/retrieve/pii/S0888327020308098

46. Gryboś R. Dynamika maszyn wirnikowych. Warszawa: Wydawnictwo Naukowe PWN; 1994.
47. Muszyńska A. Rotordynamics. Boca Raton: Taylor & Francis Group, LLC; 2005.
48. Rao JS. Vibratory condition monitoring of machines. 2000.
49. Alauze C, Der Hagopian J, Gaudiller L, Voinis P. Active balancing of turbomachinery: application to large shaft lines. J Vib Control [Internet]. 2001 Feb 19;7(2):249–78. Available from: http://journals.sagepub.com/doi/10.1177/107754630100700207
50. Bai X, Tao T, Gao L, Tao C, Liu Y. Wind turbine blade icing diagnosis using RFECV-TSVM pseudo-sample processing. Renew Energy [Internet]. 2023;211(April):412–9. Available from: https://doi.org/10.1016/j.renene.2023.04.107
51. Lagdani O, Tarfaoui M, Nachtane M, Trihi M, Laaouidi H. Numerical investigation of ice accretion on an offshore composite wind turbine under critical loads. Int J Energy Res. 2021;45(3):4112–32.
52. Okulov V, Kabardin I, Mukhin D, Stepanov K, Okulova N. Physical de-icing techniques for wind turbine blades. Energies. 2021;14(20).
53. Wang Z. Recent progress on ultrasonic de-icing technique used for wind power generation, high-voltage transmission line and aircraft. Energy Build [Internet]. 2017;140:42–9. Available from: http://dx.doi.org/10.1016/j.enbuild.2017.01.072
54. Wei K, Yang Y, Zuo H, Zhong D. A review on ice detection technology and ice elimination technology for wind turbine. Wind Energy. 2020;23(3):433–57.
55. Daniliuk V, Xu Y, Liu R, He T, Wang X. Ultrasonic de-icing of wind turbine blades: Performance comparison of perspective transducers. Renew Energy [Internet]. 2020;145:2005–18. Available from: https://doi.org/10.1016/j.renene.2019.07.102
56. Wang Y, Xu Y, Huang Q. Progress on ultrasonic guided waves de-icing techniques in improving aviation energy efficiency. Renew Sustain Energy Rev [Internet]. 2017;79(March 2016):638–45. Available from: http://dx.doi.org/10.1016/j.rser.2017.05.129
57. Wang Y, Xu Y, Lei Y. An effect assessment and prediction method of ultrasonic de-icing for composite wind turbine blades. Renew Energy [Internet]. 2018;118:1015–23. Available from: https://doi.org/10.1016/j.renene.2017.10.074
58. ISO 1940-1 Mechanical vibration - balance quality requirements for rotors in a constant (rigid) state. Part 1: Specification and verification of balance tolerances. 2003.
59. Le B, Andrews J. Modelling wind turbine degradation and maintenance. Wind Energy. 2016;19(4):571–91.
60. Alsabagh ASY, Tiu W, Xu Y, Virk MS. A review of the effects of ice accretion on the structural behavior of wind turbines. Wind Eng. 2013;37(1):59–70.
61. Pojmański G. Opinia dotycząca zagrożeń związanych z eksploatacją i awariami turbin wiatrowych Streszczenie [Internet]. Available from: http://www.sndb.pl/wiatraki/dokumenty.html
62. Fang C, Cui L. Reliability evaluation for balanced systems with auto-balancing mechanisms. Reliab Eng Syst Saf [Internet]. 2021;213(December 2020):107780. Available from: https://doi.org/10.1016/j.ress.2021.107780
63. Dalmazzo Sanches F, Ap Cavallini A, Steffen V. Theoretical and experimental applications of a rotor balancing technique without using trial weights based on augmented Kalman filter. Mech Syst Signal Process [Internet]. 2024;208(December 2023):111066. Available from: https://doi.org/10.1016/j.ymssp.2023.111066
64. Sun X, Chen Y, Cui J. A Balancing method for multi-disc flexible rotors without trial weights. Energies. 2022;15(14).
65. Yun X, Mei X, Jiang G, Hu Z, Zhang Z. Investigation on a no trial weight spray online dynamic balancer. Shock Vib [Internet]. 2018;2018. Available from: https://pdfs.semanticscholar.org/c7bd/764cbabdc4808eaf83370682cb371b44dfe9.pdf
66. Bertelè M, Bottasso CL, Cacciola S. Automatic detection and correction of pitch misalignment in wind turbine rotors. Wind Energy Sci [Internet]. 2018;3(2):791–803. Available from: https://wes.copernicus.org/articles/3/791/2018/wes-3-791-2018.pdf
67. Zhang Y, Cheng M, Chen Z. Load mitigation of unbalanced wind turbines using PI-R individual pitch control. IET Renew Power Gener [Internet]. 2015 Apr;9(3):262–71. Available from: https://ietresearch.onlinelibrary.wiley.com/doi/10.1049/iet-rpg.2014.0242
68. Rumin R, Bergander M, Cieslik J, Kulpa M. Extended active vibration control for wind turbines. 2017 13th Int Conf Perspect Technol Methods MEMS Des MEMSTECH 2017 - Proc. 2017;38–40.
69. Rumin R, Cieślik J. System for automatic rotor balancing using a continuous change of the correction mass distribution. In: Symposium A Quarterly Journal In Modern Foreign Literatures. 2010. p. 12–5.
70. Rumin R. Mathematical models of balancing rotors based on mathematical and physical relationships. Adv Sci Technol. 2011;nr 8(8):226–32.
71. Blaut J, Rumin R, Cieślik J, Hyla P, Szpytko J. Application of TKEO in the process of automatic balancing of the rotor. AUTOBUSY – Tech Eksploat Syst Transp. 2019 Feb 28;20(1–2):161–6.
72. Manufacturer of hydraulic components [Internet]. 2023 [cited 2023 Jan 12]. Available from: https://hydroleduc.com/

73. Foiles WC, Allaire PE, Gunter EJ. Review: Rotor balancing. Shock Vib. 1998;5(5–6):325–36.
74. Kim T, Na S. New automatic ball balancer design to reduce transient-response in rotor system. Mech Syst Signal Process [Internet]. 2013;37(1–2):265–75. Available from: http://dx.doi.org/10.1016/j.ymssp.2013.01.016
75. Van De Velde G, Meeus H, Verrelst B, Lefeber D, Guillaume P. Reducing the statistical scatter of automatic ball balancers using temporary speed reduction. J Sound Vib [Internet]. 2020;486:115582. Available from: https://doi.org/10.1016/j.jsv.2020.115582
76. Herzog R, Buhler P, Gahler C, Larsonneur R. Unbalance compensation using generalized notch filters in the multivariable feedback of magnetic bearings. IEEE Trans Control Syst Technol [Internet]. 1996;4(5):580–6. Available from: http://ieeexplore.ieee.org/document/531924/
77. Noshadi A, Zolfagharian A. Unbalance and Harmonic disturbance attenuation of a flexible shaft with active magnetic bearings. Mech Syst Signal Process [Internet]. 2019;129:614–28. Available from: https://doi.org/10.1016/j.ymssp.2019.04.055
78. Zhang X, Liu X, Zhao H. New active online balancing method for grinding wheel using liquid injection and free dripping. J Vib Acoust [Internet]. 2018 Jun 1;140(3). Available from: https://asmedigitalcollection.asme.org/vibrationacoustics/article/doi/10.1115/1.4037955/392561/New-Active-Online-Balancing-Method-for-Grinding
79. Hredzak B, Guo G. New electromechanical balancing device for active imbalance compensation. J Sound Vib [Internet]. 2006 Jul;294(4–5):737–51. Available from: https://linkinghub.elsevier.com/retrieve/pii/S0022460X06000253
80. Cacciola S, Riboldi CED. Equalizing aerodynamic blade loads through individual pitch control via multiblade multilag transformation. J Sol Energy Eng [Internet]. 2017 Dec 1;139(6):1–8. Available from: https://pdfs.semanticscholar.org/2aaa/e76c3bf60d549ee3dcb88568465eac251581.pdf?_gl=1*w6167d*_ga*NDEyMDcxNTE4LjE2NzI2NDYwMTE.*_ga_H7P4ZT52H5*MTY3OTMwNjEwMS4yLjAuMTY3OTMwNjE0OS4wLjAuMA..
81. Amoretti T, Huet F, Garambois P, Roucoules L. Configurable dual rotor wind turbine model based on BEM method: Co-rotating and counter-rotating comparison. Energy Convers Manag [Internet]. 2023;293(May):117461. Available from: https://doi.org/10.1016/j.enconman.2023.117461
82. Hijazi A, ElCheikh A, Elkhoury M. Numerical investigation of the use of flexible blades for vertical axis wind turbines. Energy Convers Manag [Internet]. 2024;299(November 2023):117867. Available from: https://doi.org/10.1016/j.enconman.2023.117867
83. Wang Z, Suiker ASJ, Hofmeyer H, van Hooff T, Blocken B. Coupled aerostructural shape and topology optimization of horizontal-axis wind turbine rotor blades. Energy Convers Manag [Internet]. 2020;212(April):112621. Available from: https://doi.org/10.1016/j.enconman.2020.112621
84. Hydropneumatic accumulators. Hydro Leduc; 2022. p. 36.
85. Breńkacz Ł. Bearing Dynamic Coefficients in Rotordynamics. 1st ed. Bearing Dynamic Coefficients in Rotordynamics. Hoboken, NJ, USA: Wiley; 2021.
86. Breńkacz Ł. Identification of stiffness, damping and mass coefficients of rotor-bearing system using impulse response method. J Vibroengineering [Internet]. 2015;17(5):2272–82. Available from: https://www.jvejournals.com/article/15980
87. Breńkacz Ł, Żywica G. The sensitivity analysis of the method for identification of bearing dynamic coefficients. In: Awrejcewicz J, editor. Dynamical Systems: Modelling: Łódź Poland, December 7-10, 2015 [Internet]. Cham: Springer International Publishing; 2016; 81–96. Available from: http://dx.doi.org/10.1007/978-3-319-42402-6_8
88. Breńkacz Ł, Żywica G. Comparison of Experimentally and Numerically Determined Dynamic Coefficients of the Hydrodynamic Slide Bearings Operating in the Nonlinear Rotating System. In: Volume 7A: Structures and Dynamics [Internet]. Charlotte, NC, USA: American Society of Mechanical Engineers; 2017. p. 1–12. Available from: https://asmedigitalcollection.asme.org/GT/proceedings/GT2017/50923/Charlotte, North Carolina, USA/242717
89. Lindenburg C, Winkelaar D, Hooft EL Van Der. DOWEC 6 MW PRE-DESIGN Aero-elastic modelling of the DOWEC 6 MW pre-design in PHATAS. Distribution [Internet]. 2003;(September):1–46. Available from: http://citeseerx.ist.psu.edu/viewdoc/download?doi=10.1.1.457.1123&rep=rep1&type=pdf
90. Kusnick J, Adams DE, Griffith DT. Wind turbine rotor imbalance detection using nacelle and blade measurements. Wind Energy [Internet]. 2015 Feb;18(2):267–76. Available from: https://onlinelibrary.wiley.com/doi/10.1002/we.1696
91. Zhao Y, Yang J, He Y. Preliminary design of a multi-column TLP foundation for a 5-MW offshore wind turbine. Energies. 2012;5(10):3874–91.
92. Jonkman J, Butterfield S, Musial W, Scott G. Definition of a 5-MW Reference Wind Turbine for Offshore System Development [Internet]. Journal of Offshore Mechanics and Arctic Engineering. 2009. Available from: https://www.nrel.gov/docs/fy09osti/38060.pdf
93. Torsvik J, Nejad AR, Pedersen E. Main bearings in large offshore wind turbines: Development trends, design and analysis requirements. J Phys Conf Ser. 2018;1037(4).

94. Zeillinger R, Springer H, Köttritsch H. Experimental Determination of Damping in Rolling Bearing Joints. In: Volume 5: Manufacturing Materials and Metallurgy; Ceramics; Structures and Dynamics; Controls, Diagnostics and Instrumentation; Education; General [Internet]. American Society of Mechanical Engineers; 1994. Available from: https://asmedigitalcollection.asme.org/GT/proceedings/GT1994/78873/The Hague, Netherlands/246329
95. Guo Y, Parsons T, Dykes K, King RN. A systems engineering analysis of three-point and four-point wind turbine drivetrain configuration. Wind Energy. 2013;1–20.
96. Żywica G, Breńkacz Ł, Bagiński P. Interactions in the Rotor-Bearings-Support Structure System of the Multi-stage ORC Microturbine. J Vib Eng Technol [Internet]. 2018;6(5):369–77. Available from: https://doi.org/10.1007/s42417-018-0051-2
97. Sutherland HJ. On the fatigue analysis of wind turbines. Albuquerque, NM, and Livermore, CA; 1999.
98. Orlando A, Pagnini L, Repetto MP. Structural response and fatigue assessment of a small vertical axis wind turbine under stationary and non-stationary excitation. Renew Energy [Internet]. 2021;170:251–66. Available from: https://doi.org/10.1016/j.renene.2021.01.123
99. Hyers RW, Mcgowan JG, Sullivan KL, Manwell JF, Syrett BC. Condition monitoring and prognosis of utility scale wind turbines. Energy Mater. 2006;1(3):187–203.
100. Liang Y, An Z, Liu B. Fatigue life prediction for wind turbine main shaft bearings. QR2MSE 2013 - Proc 2013 Int Conf Qual Reliab Risk, Maintenance, Saf Eng. 2013;888–93.
101. Zhang C, Chen HP, Huang TL. Fatigue damage assessment of wind turbine composite blades using corrected blade element momentum theory. Meas J Int Meas Confed [Internet]. 2018;129(March):102–11. Available from: https://doi.org/10.1016/j.measurement.2018.06.045